Monte Carlo simulation of halloysite nanotube and polyelectrolyte

Hyejeong Cheon

A thesis presented for the degree of
Master of Science

Department of Physics
Norwegian University of Science and Technology (NTNU)
Trondheim
June 2019

Abstract

Enzyme immobilization for enzymatic synthesis is commonly used for stabilizing enzymes and improving their functions. A popular methodology is the physical adsorption of enzymes on nanoscaled carriers because their large surface area allows a high loading efficiency. Some enzymes have disordered structure (intrinsically disordered protein, IDP), and for simplicity we represent these as polyelectrolytes. The chosen nanocarrier is a halloysite nanotube, which is a clay mineral that possesses a tubular structure with oppositely charged surfaces. In this work, we have used Monte Carlo simulations and a coarse-grained model to study the adsorption and conformation characteristics of an enzyme onto a halloysite nanotube. The enzyme is described as charged beads linked by harmonic bonds (polyelectrolyte). The nanotube is depicted by two types of beads constituting a positively charged inner surface and a negatively charged outer surface, and degree of ionization of surfaces is dependent on the pH. Here, we perform variation of pH and polyelectrolyte architecture. Titration curve of simulated nanotube is demonstrated to have pH-dependent characteristics. Contact probability of the polyelectrolyte in the interior of the tube shows different features from adsorption outside of the tube. Radius of gyration of the polyelectrolyte are analyzed by variations in pH and achitecture factors along the polyelectrolyte. The results demonstrate that the studied values of pH ranging from 2 to 8 affect the radius of gyration of the homogeneous polyelectrolyte, and the absolute value of net charge, the number of blocks, and the core block ratio have a significant correlation with condensation of the polyelectrolyte by statistical analysis. pH shows a significant correlation with an indicator of adsorption onto the inner surface.

Preface

This master's thesis was written to fulfill the requirements of the degree of Master of Science in Physics at Norwegian University of Science and Technology (NTNU) and handed in as a part of the course, FY3900. My project was carried out under the supervision of associate professor Rita de Sousa Dias at department of Physics.

A two-year period Was not long but I realize there have been a lot of changes in my life since I arrived in Trondheim. It was indeed a time for exploring myself, and I have met many people who are different from me. I appreciate all of them because I have learned a lot in various perspectives.

First of all, I would like to give a big thank to my supervisor, Rita de Sousa Dias, for supervising me. Your optimistic energy and curious questions make me enjoy finding solutions and inspired. The most enjoyable point with you is that I feel myself improving in many meanings, including as a scientist.

I also want to thank to Morten Stornes, Pablo Blanco Andres, Corinna Dannert, Nicholas Christiansen and Costanzt Tedesco. Your work, guidance, valuable discussion, advice and coffee breaks were helpful for me. I also thank to Peder Brenne with the administrative work.

All friends I met in department of physics, who are studying even now next to me, it was pleasant to share a study room and discuss diverse topics including science. Also, people who are supporting me, people of Slottet, Dent de Lion, and Seunghan Song who provided me the second screen, one of the biggest help for writing this thesis. I want to write down all of your names but do not since there is not enough space in this page. I would like to thank my family members and friends all over the world.

Hyejeong Cheon
Trondheim, June 2019

Table of Contents

List of Tables

List of Figures

Abbreviations

IDP	Intrinsically disordered protein
IDR	Intrinsically disordered region
MC	Monte Carlo
HNT	Halloysite nanotube
NT	Nanotube
PE	Polyelectrolyte
DNA	Deoxyribonucleic acid
RNA	Ribonucleic acid
CG model	Coarse-grained model
AA model	All-atomistic model

Chapter 1

Introduction

Enzymatic synthesis is explored in the fields of pharmaceuticals [1], purification [2, 3], and biomedical application [4] in regards to a biochemical synthesis method considering the environment. Catalytic reactions using enzymes instead of non-natural catalyst have many advantages. Firstly, it is eco-friendly with less by-products to deal with in waste treatment. Secondly, on a functional perspective, it has been found that enzymes have a higher selectivity and specificity than conventional metal-mediated and inorganic chemical catalysts, and from a biotechnological point of view, enzymes have potentiality to be explored not only *in vitro* but also *in vivo* processes [5, 6].

The activation of enzymes takes place in an organism, which means that an environment with similar conditions as the organisms is necessary for activation. In other words, enzyme synthesis in non-natural environments requires conditions such as temperature or acidity similar to the environment of their natural occurence. Furthermore, consideration of external substances that facilitate the binding of the substrate is required, which makes the use of enzymes outside the organisms challenging. In addition, enzymes can loose their function for many reasons, for example, substrates or products interfering with enzymes functionalizing or self-degradation (autolysis). Therefore, methodology for stability and preventing malfunction is required. There are methods widely used for stabilizing enzymes, such as surface immobilization including adsorption [7], covalent binding [8] and encapsulation [9, 10, 11, 12]. Of these methods, physical adsorption is widely used, requiring characteristics of a high surface area for high loading efficiency as a carrier. In this

regard, studies of nanocarrier-enzyme complexes have been actively conducted. Nanocarriers with features such as reusability, biocompatibility, large surface area and loading capacity can be considered to have potential in terms of efficiency and function [13, 14, 15].

In this regard, halloysite nanotube (HNT) can be a good candidate because of a high surface area to volume ratio, good biocompatibility, and large ability of loading. HNT is a clay mineral compound with nanoscale dimensions and special surface properties. HNT has potentiality for surface modification for enzyme immobilization as it has characteristics that can easily be functionalized with hydroxylgroup (-OH) on the outer surface. The HNT has electrical/chemical pH dependent properties on the both tube surfaces and with oppositely charge. Different chemical composition of the outer surface and inner lumen gives HNT the unique property of possessing. This suggests the potential for using halloysite in surface immobilization by selective adsorption of proteins [16, 17, 18]. In fact, experiments have been shown that a HNT is an effective carrier for protein immobilization [19].

Proteins, on the other hand, can be expressed as polyelectrolyte (PE) in the sense that the mentioned enzyme is a chain that charges in a linear structure of a polypeptide without the three-dimensional structure. Considering repeated chain of amino acid as segments in a polypeptide, we can define an enzyme as a PE. Especially, proteins that function as enzymes that have a simple linear structure rather than having a tertiary, quadratic, 3D cube structure are called intrinsically disordered proteins (IDPs). In other words, when evaluating protein immobilization through HNT as a carrier, if this protein is considered as an IDP, the topic is represented as the evaluation of a system with a PE and HNT.

Molecular simulation techniques are good tools to study interactions of macromolecules with surfaces and to predict how chemical/physical composition of modeled system affects the systems. Through modeling and simulation of HNT, research has been carried out on the perspective of electrostatic interaction [20], and spiral structure [21].

In this work, HNT and PE implemented as a coarse-grained model, and the system evaluated from the perspective of PE's conformation and adsorption. The PE is described as charged beads linked by harmonic bonds, and the HNT is depicted by two types of beads constituting a positively charged inner surface and a negatively charged outer surface where fractional charges are dependent on the pH. The model is simulated using the Monte Carlo (MC) method, and as a result, the properties of a pH-dependent nanotube are identified as well as the PE characteristics.

Changes in the distribution of radius of gyration and end-to-end distance with variations in pH were analyzed and a discussion is included regarding results of how the PE adsorbs on the HNT's outer surface and inner surface, respectively. In particular, in the case of adsorption, an analysis focused on the structure of the chain and the strength of adsorption was reported, and interestingly, formation of kinetic trap was observed simultaneously. To analyze the effect of various factors on the conformation of PE, correlations were evaluated between conformational/adsorptional indicators and chosen variables of PE architecture.

The main goal of this thesis is to investigate PE interactions with HNT and assess the applicability of HNTs as nanocarriers in enzymatic synthesis.

Chapter 2

Basic Theory

2.1 Proteins as polyelectrolytes

Polyelectrolytes (PEs) are defined as polymers with basic units that contain ionizable groups, which means they are macromolecules that become charged in aqueous solutions. PE can represent several biomacromolecules as, for example, proteins consisting of amino acids and DNA (deoxyribonucleic acid) or RNA (ribonucleic acid) strands consisting of nucleic acids [22].

When synthesized (translated) proteins have a linearly sequential structure (primary structure) of peptides, but often adopt a functional three-dimensional structure after modification processes such as glycosylation, disulfide bond (S-S) formation, and folding. The stereoscopic structure of proteins is closely related to their function, and therefore, the study of the primary, secondary, tertiary and quadratic structure of proteins is very important in researching function of proteins. However, some proteins are entirely, or in part, structurally disordered, especially enzymes related to membrane signalling. These proteins take advantage from the disordered structure using it to bind to multiple substances with various structures, which means they are multifunctional. Without three-dimensional structure known as main feature of most of proteins, proteins functionally perform with disordered part, and these proteins are called intrinsically disordered protein (IDP), or natively unfolded proteins. Regions of proteins with deficient 3D structure are called intrinsically disordered region (IDR) [23, 24, 25].

2.2 Halloysite nanotube

Halloysite nanotube (HNT) is an aluminosilicate compound found in clay material. It is a layered silicate material with a chemical composition similar to kaolinite. Both kaolinite and halloysite have crystallographic structures with a combination of tetrahedral silica and octahedral alumina, arranged in a planar sheet. However, in case of halloysite, water exists between the tetrahedral and octahedral sheets. Therefore, a chemical composition of kaolinite is $Al_2(OH)_4Si_2O_5$, and halloysite is $Al_2(OH)_4Si_2O_5 \cdot nH_2O$ as the hydrated form with n number of water molecules. The number of water molecules determines a distance between rolled layers in halloysite and it is denoted as, for example, $Al_2(OH)_4Si_2O_5 \cdot 2H_2O$ for halloysite-7Å [18, 26].

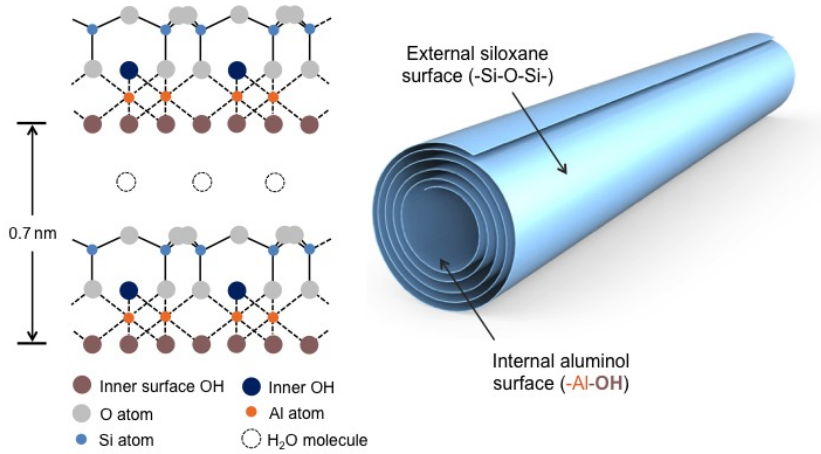

Figure 2.1: Schematic description of HNT (halloysite-7Å). Image is adapted from Phantom Plastic.

In two structures mentioned above, an apical oxygen of tetrahedral silica (SiO_4) is shared by octachedral alumina (Al_2O_3). Here, a lattice mismatch of different structures induces the transformation of the structure and HNT in particular, adopts a tube-shaped structure. Water molecules between layers form hydrogen bonds with other water molecules or surfaces of halloysite, and these bonds compensate the stress of mismatch. Therefore, rolled silica sheet is inside tube and alumina sheet is outside the tube. This is shown in figure 2.1.

Because of this specific structure, halloysite nanotubes have different chemical prop-

erties on the outside and inside, which are determined by the nature of alumina and silica respectively. HNT has a large number of functional sites, which can be seen as an aluminol group (Al−OH) inside and a silanol (Si−OH) outside as shown in figure 2.1. Silicon has higher electronegativity than aluminum (1.90 > 1.61) [28], so the two surface groups differ in the degree of protonation in aqueous solution, as confirmed by the different acid dissociation constant (pK_a). Therefore, the outer silanol gets a negative charge when it dissociates, and the aluminol gets a positive charge upon protonation. In other words, each surface has acidic or basic properties in one nanotube compound, which shows why halloysite has an acid-base bifunction, that is, it is amphoteric in nature.

2.3 Monte Carlo simulation

Monte Carlo method is a computational methodology based on repeated random sampling to get statistical result. There are a lot of examples of molecular simulations which utilize Monte Carlo method such as simulating nanoparticles [29] or DNA condesation [30]. In molecular simulation

In molecular simulations, a process of random sampling means choosing a random configuration of molecules in a system. Coordinates of particles which exist in a system are translated, and by this movement, new coordinates are adopted, or not. Accepting or rejecting a new configuration is determined by a specific criteria, which is called the Metropolis algorithm. By the Metropolis selection criterion, acceptance or rejection of a new configuration is decided. Through successive trial moves, properties of the system converges towards its equilibrium average value.

Metropolis Monte Carlo algorithm

A trial move which is randomly generated is accepted if the system is qualified by the Metropolis criterion, and in molecular simulation, the criterion is based on the potential energy term with the Boltzmann factor according to the following equation,

$$\frac{P(U_{n+1})}{P(U_n)} = \exp\left(\frac{-(U_{n+1} - U_n)}{k_B T}\right) \tag{2.1}$$

where U_n is a potential energy of the nth configuration, k_B is the Boltzman constant and T is the temperature of system. Therefore, there are three possible options for accepting/rejecting new configuration:

1. $U_{n+1} < U_n$: New state is accepted and previous state is replaced by new state.

2. $\exp\left(\frac{-(U_{n+1}-U_n)}{k_B T}\right) \geq R$: Energy of the new state is higher than the previous state, but the energy difference is small enough to be accepted probabilistically. This is expressed by random number, R. New state is accepted.

3. $\exp\left(\frac{-(U_{n+1}-U_n)}{k_B T}\right) < R$: Energy of the new state is higher than the previous state, and the energy difference is large enough to be rejected probabilistically. This is expressed by random number R. New state is rejected.

After a large number of trial moves (also called steps), a property of the system (*i.e.* U) converges. The simulation run of converging to a specific state through repetition of steps is called an equilibrium run, which assumes that the state of equilibrium is reached. Afterwards, another run is performed to obtain the statistical value of the properties of interest, and this is called a production run. Average of all possible states of a system during production runs is called an ensemble average.

2.4 Coarse-grained model

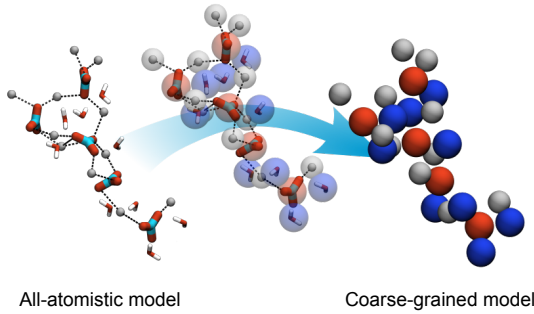

Figure 2.2: Schematic representation of coarse-grained (CG) model and all-atomistic (AA) model. Image is adapted from [31].

Coarse-grained (CG) models are computational models that mimic the behaviour of a complex system by discretizing it into simpler sub-components. The extent to which the system is discretizing reflects the degree of granularity of the model. Therefore, a model can be defined according to how large granularity of it has. A model that describes a molecule with its atoms is called an all-atomistic (AA) model, as shown in figure 2.2. In molecular simulations, the calculation time is often coupled to the number of particles in the system, which means coarse-graining reduces the time it takes to run the simulation. On the other hand, more elaborate and discrete models give more details and the more accurate results that are, in principle, close to the reality.

Chapter 3

Methods

3.1 System

Systems containing a HNT and a PE are modeled in this work. The dimensions of the HNT were chosen according to published data from experimental results of studying molphology of HNT by AFM and TEM [26]. Here the referenced parameters are the tube internal radius (d), the external radius (D), the length (L) of the NT, and the acid dissociation constant (pK_a) to determine weak basicity and weak acidity of the inner and outer surfaces.

Table 3.1: Dimensions of HNTs found in two different regions from New Zealand [32] and USA [33].

Region	d [Å]	D [Å]	T [Å]	L [Å]
Northland, New Zealand	80-260	190-400	80-180	1000-3000
Dragon Mine, Utah, USA	50-300	200-1500	50-500	500-15000

Because HNTs are mineral compound that can be found in mud, their dimensions varied with the region they were found in. Some examples can be found in the table 3.1. Based on the examples found in USA and New Zealand (table 3.1), the following parameters were chosen: D = 300 Å, d = 60 Å, which results T = 240 Å, and L = 240 Å. HNTs actually have spiral-rolled structures with several layer, but here a HNT is generated as a continuous tube (cylindrical structure) without rolled edges on the inner and outer surfaces. The simulation cell in which the tube is generated was a cylinder with a radius of

800 Å and a length of 1300 Å considered large enough to prevent strong wall effects.

pK_as (acid dissociation constants) of alumina and silica can be determined regarding the structure of halloysite. Halloysite is a mineral compound with monoclinic crystal structure with repeating unit of $Al_2(OH)_4Si_2O$. Surfaces of HNT possess a hydroxyl functional groups (−OH) exposed to aqueous solution [18, 20]. The outer surface of HNT is composed of silica (SiO_2) (strictly specifying, siloxane (Si−O−Si)), and silanol (Si−OH) groups. In equilibrium state, pK_a from protonation/deprotonation processes is obtained from

$$-\mathrm{Si}-\mathrm{OH} + \mathrm{H_2O} \overset{K_a}{\rightleftharpoons} -\mathrm{SiO^-} + \mathrm{H_3O^+} \tag{3.1}$$

$$\mathrm{p}K_a = -\log_{10} K_a = -\log_{10} \frac{[\mathrm{SiO^-}][\mathrm{H_3O^+}]}{[\mathrm{SiOH}]} \tag{3.2}$$

Here, we use pK_a = 4.23 for groups on the silica surface taking into account the values found in the literature based on experimental results of measuring proton binding affinity of HNTs [18].

On the other hand, the inner surface of halloysite is composed of alumina (Al_2O_3), and aluminol (Al−OH) groups of the inner surface dissociate in the aqueous solution as below.

$$-\mathrm{Al}-\mathrm{OH} + \mathrm{H_2O} \overset{K_a}{\rightleftharpoons} -\mathrm{AlOH_2}^+ + \mathrm{OH^-}$$

$$\mathrm{p}K_a = -\log_{10} K_a = -\log_{10} \frac{[\mathrm{AlOH_2^+}][\mathrm{OH^-}]}{[\mathrm{AlOH}]}$$

Here, we use pK_a for alumina as 9.22 from experimental results of acid-base titration of alumina by Morel and co-authors [34].

A PE here is represented as a simple chain which mimicks an IDP. In this study, the system was constructed taking into account a polypeptide simple linear and charged, rather than a protein with a complex structure, for example, HSP12, one type of heat shock proteins, has a structure of alpha-helix at residues 71-109 but is disordered at residues 1-70 [35]. Future research may consider the protein which presents both IDR and non-IDR together in its structure.

Among the 20 amino acids that make up the actual IDP, the charged amino acids that may be present in a protein, some are negatively charged: Aspartic acid (Asp, pK_a 3.65),

and Glutamic acid (Glu, pK_a 4.25). Side groups of these amino acids whose pK_a's are low enough to lose proton, and consequently a polypeptide chain which is made up of these amino acids is negatively charged. On the other hand, some amino acids side chains have positive charges, and a basic nature: Arginine (Arg, pK_a 12.5), Histidine (His, pK_a 6.0), and Lysine (Lys, pK_a 10.53). The pKas are high enough that protons bind to these groups, leading a positive charge on the amino acid [36].

For simplicity, all monomers in the modeled protein were considered strongly charged (either positive or negative), that is, they are insensitive to charges in pH unlike amino acids. Therefore, this study does not represent one specific existent IDP's behavior as enzyme. However, about 10 percent of all proteins are fully disordered, literally IDP, and about 40 percent of eukaryotic proteins at least have a long chain of IDR (>50 amino acids) [35, 37]. Furthermore, as Glutathione, a tripeptide with three amino acids; Glutamic acid, Cysteine and Glysine [38], this infers there can be a short and simple polypeptide made up of charged amino acids. Judging from this fact, this study is not a simulation result modeled after a specific IDP that actually exists, but it can be expected that the results give a contribution as a preliminary results considering subsequent simulations of IDPs afterwards.

3.2 Modeling

A hard-sphere CG model is implemented here for a system of a HNT, a charged PE and counterions in a salt-free system. This system is modeled and simulated considering the canonical ensemble, with conserved number of particles, volume, and temperature (NVT). The primitive model is used, which describes the particles as hard spheres with point charges in the center. The solvent is described by a continuum with a dielectric constant $\epsilon_r = 78.2$, that of water at $T = 298K$, the temperature used in the simulations.

Halloysite nanotube

The HNT is composed of two types of coarse-grained hard sphere (beads) which are here named alumina and silica groups. The alumina groups have a 2.0 Å radius, valency $z = +1$ and pK_a = 9.22, as mentioned. Total number of alumina groups is 100, which gives a surface charge density (σ_{in})

$$\sigma_{in} = \frac{+1 \cdot 100 \cdot 1.602 \cdot 10^{-19}}{2\pi \cdot 60 \cdot 700} = 6.07 \cdot 10^{-3} = 6.07 \text{ mC/m}^2 \tag{3.3}$$

Experimental results of measuring surface charge density of alumina from Yin and co-workers [17] show approximately 6 mC/m^2 for alumina and -11 mC/m^2 for silica surface charge density under conditions of pH 3 to 8, considering both surfaces are fully charged. Here, we consider surface charge of inner surface is neutralized by the outer surface, so σ_{out} is -6.07 mC/m^2 by silica beads. Therefore, coherent number of silica beads is 500. Silica beads also have 2.0 Å as radius but -1 valency and pK_a = 4.23. The alumina and silica surface groups are generated at the inner and outer surface of a HNT which is impenetrable to all particles (PE monomer and small ions). The alumina and silica surface groups are also kept fixed throughout the simulations. Both alumina and silica groups have counterions (ions with opposite charge) with the same radius, 2.0 Å.

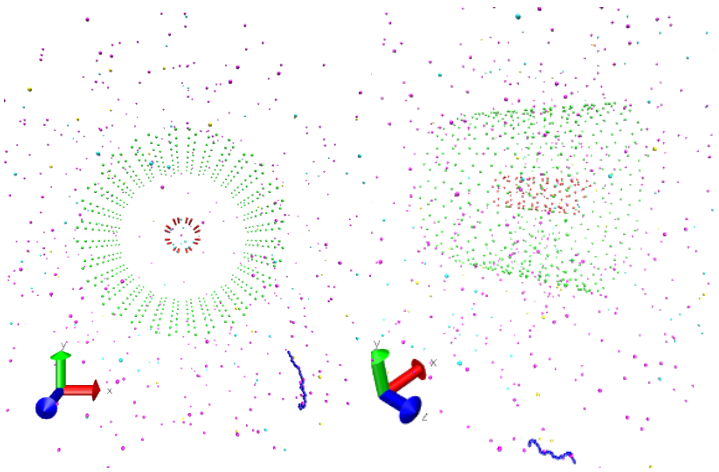

Figure 3.1: Representative snapshots of a system of HNT and PE.

Polyelectrolyte

A PE chain is described by monomers (hard sphere beads) with radius 2 Å. The monomers are positively or negatively charged and we denote a chain with all positively charged monomers as a positively charged PE chain, and the opposite for a negatively charged

PE chain. The monomer charge is not sensitive to pH variations, that is the charges are fixed, as opposed to the surface groups in the HNT. The chain here is considered a semi-flexible chain. Monomers in a chain are connected by harmonic bonds with the chain flexibility controlled by harmonic bond and angular energy (see next section). counterions of monomers are presented as hard sphere beads, with the same number of and opposite charge to the monomers with radius 2 Å.

Modeled system of a HNT and a PE with counterions is shown in figure 3.1.

Potential energy

All interactions are taken as pair-wise additive. The total potential energy of a system (U) is calculated according to

$$U = U_{\text{nonbond}} + U_{\text{bond}} + U_{\text{ang}} \tag{3.4}$$

depicting all different contributions to the potential energy of the system. Potential energy from non-bond interactions is the combination of two potential energy terms. These two are the electrostatic potential energy between particles and the hard-core repulsion given by

$$U_{\text{el,hc}} = \sum_{i<j} u_{ij}(r_{ij}) \tag{3.5}$$

where the summation extends over all particles with u_{ij} defined as

$$u_{ij} = \begin{cases} \infty, & r_{ij} < R_i + R_j \\ \\ \dfrac{q_i q_j}{4\pi\epsilon_0\epsilon_r r_{ij}}, & r_{ij} \geq R_i + R_j \end{cases} \tag{3.6}$$

with r_{ij}, the separation distance between two ith and jth particles. R_i denotes the radius, q_i the point charge and z_i the valency of a particle i. e is the elementary charge, $1.602 \cdot 10^{-19}$ C. ϵ_0 is the vacuum permittivity, $8.854 \cdot 10^{-12}$ Fm^{-1} and $\epsilon_r = 78.2$ is the dielectric constant of the medium, here takes as water at a temperature of 298 K.

The bond potential energy between two monomers in a chain is given by

$$U_{\text{bond}} = \frac{k_{\text{bond}}}{2} \sum_{i=1}^{N_{\text{bead}}} (r_{i,\text{bond}} - r_{0,\text{bond}})^2 \tag{3.7}$$

where the force constant for the bond potential (k_{bond}) is 2.409 kJmol^{-1}, and the equilibrium separation for the bond potential ($r_{0,\text{bond}}$) is 5.0 Å. The angular potential energy is given by

$$U_{\text{ang}} = \frac{k_{\text{ang}}}{2} \sum_{i=1}^{N_{\text{bead}}} (r_{i,\text{ang}} - r_{0,\text{ang}})^2 \tag{3.8}$$

where the force constant for the angular potential (k_{ang}) is 0.001 kJmol^{-1}, and the equilibrium angle for the angular potential ($r_{0,\text{ang}}$) is 180°.

During the simulation the surface groups of the HNT dissociate, which leads to a change in the potential energy. The acceptance of each ion association/dissociation (protonation/deprotonation) by charge-change move is related to the Metropolis selection criterion by ΔU. The probability that surface group will have a charge is given by the potential energy difference,

$$\Delta U = \Delta U_{\text{el}} + k_B T \ln 10(\text{pH} - \text{pK}_a)\Delta z \tag{3.9}$$

where k_B is the Boltzmann constant, $1.38 \cdot 10^{-23}$ JK^{-1}, T is the temperature, 298 K, and here, pK_{a} for alumina groups is 9.22, and 4.23 for silica as described previously. Δz as the change of valency of each surface groups.

Both pH and pK_{a} are inputs in the program, and the HNT ionization (degree of ionization) is calculated according to

$$\alpha = \frac{\sum_{i=1}^{N} |z_i|}{N} \tag{3.10}$$

where N is the number of silica or alumina surface groups.

ΔU_{prot} is governed by pH of the system and the pK_{a} of each surface groups. This is described by

$$\Delta U_{\text{prot}} = k_B T \ln 10(\text{pH} - \text{pK}_a)\Delta z = \pm k_B T \ln 10(\text{pH} - \text{pK}_a)z \tag{3.11}$$

wherethe sign (±) is related to the surface groups which are protonated (+) and deprotonated (-). At a given step, each surface group is neutral or charged with oppositely charged

counterions corresponding surface groups for electroneutrality of the system.

Therefore, the probability of accepting or rejecting a configuration with switching on or off of surface group's charge is governed by ΔU_{prot}. As a result, α can be obtained by calculation of number of charged surface groups and counterions, respectively.

3.3 Implementation

MOLSIM software

We used the molecular modeling package MOLSIM, software version 6.4.2, developed by Linse and co-workers [39]. This is an integrated program for molecular dynamics (MD), Brownian dynamics (BD), and Monte Carlo (MC). Different types of simulation cells can be chosen in MOLSIM, for example, cubic, cylindrical or spherical cells [39].

In practice, the first configuration is generated by MOLSIM and subsequent runs are followed as accepting new configurations. The run for a system reaches to an equilibrium state is called an equilibrium run. Following runs utilize the final configuration from the equilibrium run as the first configuration for measuring a property of interest in the equilibrated state. This calculation is used as a production run, and consequently statistical results from the production run are calculated and plotted.

Here, we use the Monte Carlo method for a system in the canonical ensemble (NVT), in a cylindrical cell without periodical boundary conditions. MOLSIM works in a sequencial work-flow, as shown in figure 3.2.

(1) First, the input file is read and all variables are checked for consistency, for example, electroneutrality of the system. The number of attempted moves (steps) is decided by the user in the input also. The number of steps is divided into microsteps and macrosteps. (2) Then, the first configuration is generated. (3) MC procedure is initiated and trial moves of the particles are attempted, (4) and new configurations are accepted or rejected according to energy arguments, as explained previously. After finalizing sampling variables after specified number of microsteps, each macrostep is completed calculating the averaged variables, and they are written in output file. (6) Finally, average over all macrosteps are calculated.

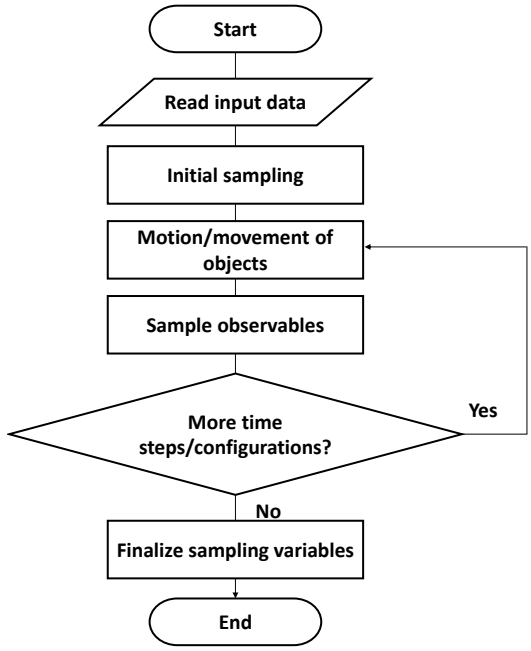

Figure 3.2: Illustration of flow chart of MOLSIM software.

We implemented 10 macrosteps for an equilibrium run, and a macrostep includes 10,000 microsteps. Totally, $10 \cdot 10,000$ steps for an equilibrium run. Production run is carried out with 20 macrosteps which consist of 20,000 microsteps each, so $20 \cdot 20,000$ for a production run. The statistical results that we discuss here are averaged after whole 20 macrosteps are done, as an ensemble average.

Trial moves

A selection of trial moves is available in MOLSIM package, and four types of trial moves have been used in this work: (1) single-particle translation, (2) translation and (3) pivot rotational move of a chain, and (4) a charge-change move.

(1) The translational move of a single particles was applied to all particles except alumina and silica surface groups. The maximal translational displacement of a particle along

one axis is 2.5 Å for a monomer in a PE chain and 12.5 Å for counterions.

(2, 3) The translational move of a chain is carried out with the maximal translational displacement of 1.5 Å and the pivot rotational move of a chain is done by the maximal rotational displacement of 22.5°.

(5) The charge-change move is only applied on the weakly charged surface groups, alumina and silica, and corresponds to switching on or off the charge of a counterion. For example, in protonation process, z becomes +1 for alumina, and z becomes 0 for silica ($z \rightarrow z + 1$), and in deprotonation process, z becomes 0 for alumina, and z becomes -1 for silica ($z \rightarrow z - 1$).

How often a move is applied depends on which type of trial move it is. Simple particle moves (1, 2) are attempted 10 times more often than the other two (3, 4).

Studied systems and variables

To assess the effect of pH on the interaction of a HNT and a negative and positively charge PE, we run various systems. Furthermore, systems including variations of the architecture of PE were also studied to assess how each feature of PE affects its conformation and adsorption to the HNT by statistical analysis. The studied variables were

(1) Number of blocks, N_{block}, refers to the number of section in the PE with sequencial monomer of one type; For example, a diblock copolymer has 2 blocks and a homogeneous PE has only 1 block.

(2) Net charge, Z_{net} is defined as $N_{\text{mon}}^{\text{pos}} - N_{\text{mon}}^{\text{neg}}$, so if the number of positive monomers is the same as the negative ones, then net charge becomes 0. However, if $N_{\text{mon}}^{\text{neg}} > N_{\text{mon}}^{\text{pos}}$, the net charge becomes negative.

(3) Absolute value of net charge, regardless of the sign of net charge, $|Z_{\text{net}}|$.

(4) The number of monomers is the number of hard sphere beads which make

a PE chain, N_{mon}.

(5) Core block ratio, R_{core}, is the ratio between the number of monomers in the center block and the total number of monomers in the chain. For example, in a triblock copolymer with three blocks (neg-pos-neg) of equal length, the core ratio is $1/3 = 0.333$. However, if a chain doesn't have a center of symmetry, then it becomes zero. This value is for evaluating the distribution of charge throughout the chain simply. This useful when distinguishing two PEs such as (neg-pos-neg) triblock-PE with (10-10-10) number of monomers and (pos-neg-pos) triblock-PE with (5-20-5) number of monomers, because other factors can not classify them.

Table 3.2: Table of variables for simulations of different systems. pH is an integer variable in a range of 2 to 8. For example, the first row corresponds to two systems with 1 block (homogeneous PE) and 40 monomers each, defining a positive and negatively charged chain.

N_{block}	N_{mon}	Z_{net}	$\lvert Z_{net}\rvert$	R_{core}	pH
1	40/40	40/-40	40/40	1/1	2-8
2	30/40/60/60	-10/-20/0/20	10/20/0/20	0/0/0/0	2-8
3	20/30/30/40/40	0/-10/-10/-20/-20	0/10/10/20/20	0.5/0.67/0.33/0.25/0.075	2-8
4	40	0	0	0	2-8
6	60	0	0	0	2-8

pK_a alumina = 9.22
pK_a silica = 4.23

Table 3.2 summarizes all 91 systems calculated during this work, including tested variables. In all these systems, PE is generated in a random location in the cylindrical cell. A system of a PE generated in the lumen is not considered for statistical analysis. 40-bead PE with negative and positively charge in the absence of HNT were also calculated.

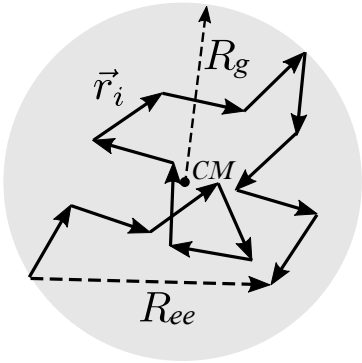

Figure 3.3: Description of R_g and R_{ee}. Each position vector is $\vec{r}_i$ and CM denotes the location of the center of mass in a PE chain. Image is adapted from [40] and redrawn.

3.4 Analysis

3.4.1 Structural analysis

Radius of gyration (R_g) and end-to-end distance (R_{ee})

To evaluate conformations of a PE in this study, properties such as the distributions of (1) the end-to-end distance (R_{ee}) and (2) the radius of gyration (R_g) are studied. The conformation is the description of a polymer as a spacial structure determined by the relative locations of all monomers [41]. The end-to-end distance is described by the distance between two ends of a chain, the first monomer and the last monomer. The radius of gyration is the average distance between the center of mass and each monomer in the polymer. Both are described in figure 3.3. The ensemble average of these quantities are given by mathematical expressions,

$$\left\langle R_g^2 \right\rangle = \frac{\left\langle \sum_{i=1}^{N} |\vec{r}_i - \vec{r}_{CM}|^2 \right\rangle}{N} \tag{3.12}$$

$$\left\langle R_{ee}^2 \right\rangle = \left\langle |\vec{r}_N - \vec{r}_1|^2 \right\rangle \tag{3.13}$$

where $\vec{r}_i$ is the position vector of ith monomer, $\vec{r}_{CM}$ is the position vector of the center of mass, N is the number of monomers in a PE chain, and the angular brackets $\langle ... \rangle$ denotes the ensemble average. When we denote the average of the radius of gyration and the

end-to-end distance here, we describe them as the root-mean-square value, $\left\langle R_g^2 \right\rangle^{1/2}$ and $\left\langle R_{ee}^2 \right\rangle^{1/2}$.

The end-to-end distance and the radius of gyration of ensemble can be represented instead as probability distribution function $P(R_g)$ and $P(R_{ee})$.

Adsorption and contact analysis

Contact distance

A measure of whether a monomer or chain of the PE is adsorbed or not to the HNT can be obtained by defining a threshold distance to the surface of the tube. This distance was here chosen to be based on the Bjerrum length (λ_B), which is the distance at which the electrostatic interaction equals 1k$_/textB$T. This distance is determined by the dielectric constant of the medium (here, water) and the temperature. This is given by

$$\lambda_B = \frac{e^2}{4\pi\epsilon_0\epsilon_r k_\mathrm{B} T} \tag{3.14}$$

e is the elementary charge, ϵ_0 is the vacuum permittivity, k_B is the Boltzmann constant, T is a temperature, and ϵ_r the relative dielectric constant. Therefore 7.1 Å is the criteria for determining contact (adsorption). Monomers at a center-to-HNT surface distance shorter than 7.1 Å from the alumina groups are considered to be in contact with the inner surface, and at distance shorter than 7.1 Å from the silica groups indicates adsorption at the outer surface. If there is at least one monomer within the adsorption threshold, the PE chain is assumed to be adsorbed. In other words, a contact probability can be obtained for each monomer of PE, and each contact distribution can be evaluated independently the internal surface (P_{in}), from the external surface (P_{out}) and both of them (P_{in+out}).

Loops, tails, and trains analysis

Based on the above contact criteria, loops, tails, and trains analysis can be performed when analyzing adsorbed PE chain. The number and length of each loop, tail, and train, and number of segments in each of these are indicators that describe how the chain is adsorbed at the surfaces. Figure 3.4 shows how an adsorbed PE forms loop(s), tail(s), and train(s). A part of the chain is called train when successive segments are within the range of contact distance. If there are multiple trains in a PE chain, segments between one train

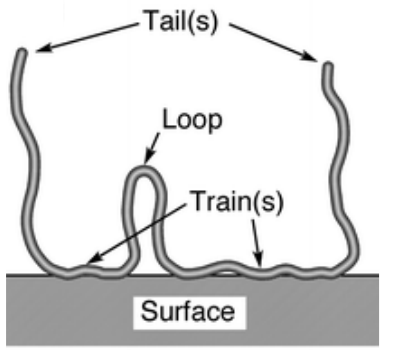

Figure 3.4: Description of a surface-adsorbed PE with loop(s), tail(s) and train(s). Image and caption are adapted from Araki with permission.

and the other train that are not contact with the surface form a loop. In other words, if both ends of a segment, which is not in contact, are in contact, this part is called loop. If only one of the tube ends of the segment is in contact, this is called a tail [43].

3.4.2 Statistical analysis

Following statistical analyses were performed to evaluate correlation of variables. Here, analyses were implemented by IBM SPSS software version 24 [44].

Basic of Statistics

In statistics, variables can be divided into two types, depending on whether we can adjust them or not. Variables that can be varied intentionally are called independent variables. These are sometimes referred to as explanatory or predictor variables. On the other hand, dependent variables are variables that we obtain as a result. Dependent variables are what we want to know how are changed at a variation of independent variables. An analysis method that identifies the relationship of variables or estimates values through a given sample by statistics is called a statistical analysis.

The statistical analysis is based on hypothesis test. Hypothesis testing generally assumes that the tested variable follows a particular probability distribution. Most commonly

used distributions are normal and t-distribution, and in hypothesis tests for variance, χ^2-distributions or F-distribution are mainly used, but here we do not explain each distribution in detail.

Null hypothesis, alternative hypothesis and significance level are needed to be known for hypothesis testing. Null hypothesis (H0) refers to a hypothesis that is a specific statement that we want to test directly, and alternative hypothesis (H1) refers to a hypothesis that is accepted when the null hypothesis is rejected.

The meaning of 'null' in a null hypothesis is a hypothesis that nullifies the argument of a counterargument. However, in general, null hypothesis is set as 'hypothesis that should be rejected' in hypothesis testing. Hypothesis testing is actually a statistical analysis that tests whether null hypothesis can be rejected or not. That is, in many cases, testers want to prove that the alternative hypothesis is true.

Significance level is the tolerance of the probability of rejecting the null hypothesis and adopting the alternative hypothesis even the null hypothesis is true. Statistically, we usually refer to it as 'significant' when it is particularly meaningful. The significance level is usually expressed as p-value, and for a typical hypothesis test, a 5% significance level is taken into account. This means that the probability of error of rejecting 'true' null hypothesis is 5% or less, that is, the test assures 95% confidence. not [45, 46, 47].

Normality test

Normality refers to a characteristic that follows a normal distribution and is symmetrical to the left and right with the mean value centered.

Whether sample data follow normality or not determines which statistical test should be applied, so before statistical testing is carried out, it is essential to ensure that the data conforms to normality. First, the histogram of the data is checked for normality, and if there is not enough data to draw the histogram, tests such as the Shapiro-Wilk test or the Kolmogorov-Smirnov are recommended. Normally, the Kolmogorov-Smirnov test is used for a large number of samples (50 or more), but this number is not precisely defined. The null hypothesis of the two tests is that 'The sample satisfies normality' and the alternative hypothesis is 'The sample does not satisfy normality'. If the significance level is lower than 0.05 then the sample will not meet its normality with a confidence of 95%.

Scatter plot

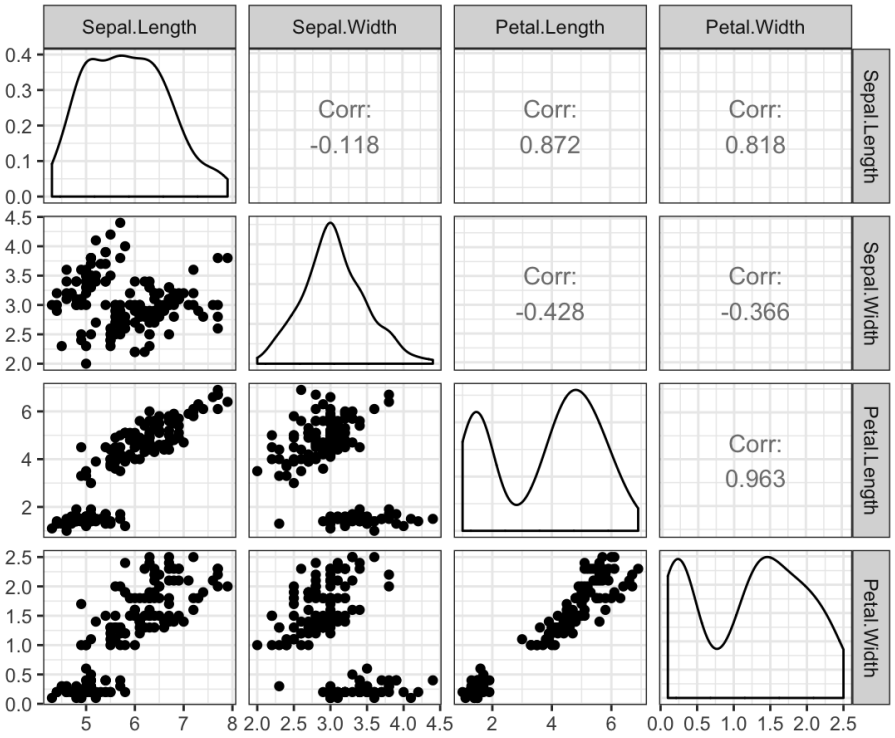

Figure 3.5: Example of multidimensional scatter plot. The sepal length, the sepal width, the petal length and the petal width are variables of interest and we can infer correlations between two of them respectively by distribution. Image is adapted from Kassambara.

A scatter plot is a plot on an orthogonal coordinate system that shows the relationship between two (or three) variables, and has the advantage of visually identifying the relationship between variables. In particular, it is essential to evaluate correlations between variables and to identify outliers. To check a correlation between multiple variables, then a multi-dimensional scatter plot is recommended. This figure has the advantage of presenting at a glance the correlation between the various variables, and is also called a scatter plot matrix, as it places the variables in rows and columns, respectively. One example of such multi-dimensional scatter plot is shown in figure 3.5. It shows the variables of interest at x and y-axe [48] and a density distribution as a histogram is also shown diagonally.

As an example, figure 3.5 shows the multi-dimensional scatter plot of features about

iris flower. There are four variables of interest, which are the sepal length, the sepal width, the petal length and the petal width. A scatter plot of the petal length and width (plot at the fourth row and the third column) shows high correlation by congested dots diagonally. Degree of correlation is also displayed as 'Corr: 0.963' on a plot located at the diagonally symmetric plot from the mentioned scatter plot, and a correlation coefficient is explained in the next section.

Spearman's rank correlation test and coefficient (Spearman's ρ, or r)

The Spearman's rank correlation coefficient is a nonparametric measure of association of two variables. That is, it evaluates how well the relationship between the two variables can be described as a monotonic function. In order to calculate ρ, ranks of two variables of interest are obtained first. Ranking in statistics refers to the data transformation of replacing numerical or ordinal values to their rank number values in ascending order by sorting. For example, the data (5.9, 5.2, 5.5) are transformed to the data (3, 1, 2), and this data made of integers are called ranks.

There are two variables (X_1, Y_1), (X_2, Y_2), ... (X_n, Y_n) in which we evaluate a correlation and ranks of these are (x_1, y_1), (x_2, y_2), ... (x_n, y_n). The difference in ranks for the ith individual is $d_i = x_i - y_i$. Spearman's rank correlation coefficient (r) for data we assess here is given by

$$r = 1 - \frac{6 \sum d_i^2}{n(n^2 - 1)} \tag{3.15}$$

where n denotes the number of individuals.

Table 3.3: Guideline for interpreting correlation coefficient [49, 50].

Coefficient	Correlation relationship strength
$\|r\| = 0.0$	No correlation
$0.0 \leq \|r\| < 0.2$	Very weak correlation
$0.2 \leq \|r\| < 0.4$	Weak correlation
$0.4 \leq \|r\| < 0.6$	Moderate correlation
$0.6 \leq \|r\| < 0.8$	Strong correlation
$0.8 \leq \|r\| < 1.0$	Very strong correlation
$\|r\| = 1.0$	Perfect correlation

This coefficient has a value from -1 to 1. The closer this value is to 0, the more it is determined that there is no correlation between two variables. The closer to -1 is

the negative correlation, that is, one variable increases as the other decreases. The positive correlation, the closer this value to +1, means one variable increases as the other increases. The correlation coefficient is interpreted according to a criteria which is listed in table 3.3 [45, 49, 50, 51].

Validity of tested coefficients is determined by p-value obtained from the test. Null hypothesis here is $r = 0$, that is, there is no correlation between two variables.', and if p-value is less than 0.05, this null hypothesis is rejected. In other words, there is a correlation between the two variables with a confidence of 95% [46, 47].

Chapter 4

Results and discussion

The goal of this study was to evaluate the potential of HNT as an enzyme carrier for enzymatic synthesis. As discussed, the enzyme is modeled simply as a PE. In order to investigate how a PE interacts with a HNT and how different factors such as,pHor N_{mon}, are related, results are divided into five sections, as follows:

1. The first section is mainly focused on NT's pH-dependent characteristic by looking at different degree of ionization the inner and outer surfaces with pH variations.

2. The second section is about one single PE generated at a random location of in the cell and the interactions of it with a NT at different pH values. This is for evaluating two main parts, one is conformation behavior of a PE, and the other is adsorption analysis of a PE onto the tube.

3. The third section is a discussion derived from results of the second section. Here, we discuss why a PE's conformation and adsorption properties are changed with pH variations.

4. The fourth section is an analysis investigating conformation and adsorption by a PE generated from the tube lumen.

5. The last section is about studying correlation of the ensemble averaged ($\left\langle R_g^2 \right\rangle^{1/2}$) and the number of adsorbed segments onto the inner and outer surfaces ($N_{\text{seg}}^{\text{ads,in}}$ and $N_{\text{seg}}^{\text{ads,out}}$) of with a PE's architecture factors and pH conditions. The goal is to find which and how factors are correlated with conformation and adsorption of a PE in a system including a HNT.

4.1 Halloysite nanotube titration behavior

The pH-dependent behavior, one of the most important characteristic of HNT, is assessed by titration curves. Titration curves of the HNT in the absence of a PE, and HNT in the presence of a negatively charged and a positively charged PE were evaluated. First, the titration curve of the HNT is described.

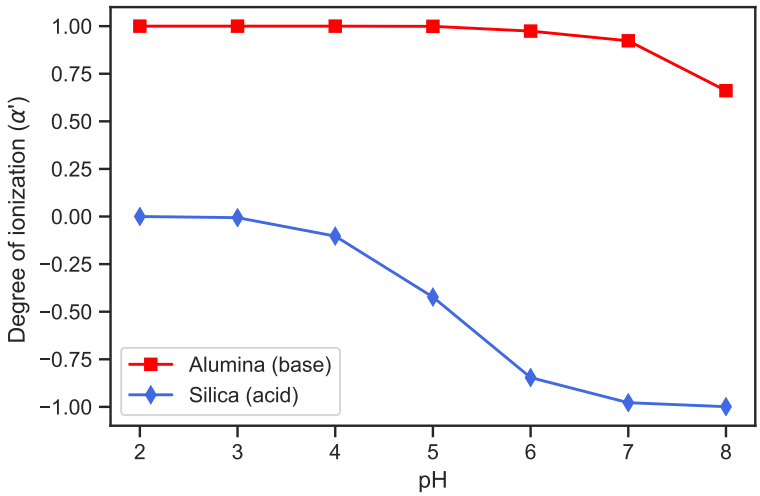

Figure 4.1: Titration curve of degree of ionization of the alumina and silica groups on simulated HNT surfaces. Meanwhile, degree of ionization (α') here is expressed with the sign of charge for comparing experimental results, so silica has negative sign.

We compare the titration curves of the simulated HNT and the experimental results from a HNT through figure 4.1 and figure 4.2. The simulation result of figure 4.1 shows degree of ionization in each surface as a function of pH. The experimental results in fig-

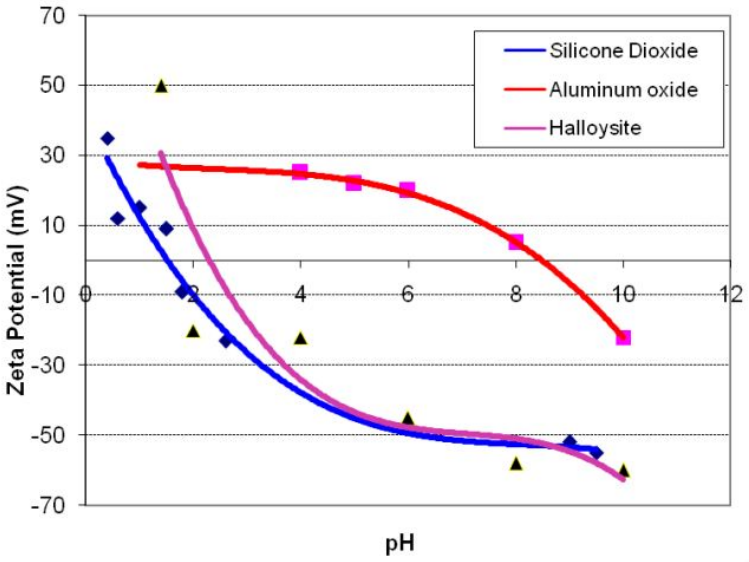

Figure 4.2: Titration curve of ζ-potential from HNT. Image is adaped from for Controlled Release of Active Agents.

ure 4.2 show titration curves of silica surface and alumina surface, respectively, evaluated in terms of the ζ-potential. The degree of ionization and the ζ-portential refer to different quantities but they have shown that both are related to the surface charge or surface group dissociation [53]. Although the two results are not exactly the same, we can analyze the similarities and differences in the titration curves of silica and alumina obtained by simulations and experiments.

In both figures 4.1 and 4.2, the titration curve of alumina (internal surface) shows a smooth decrease in both the ζ-potential and the degree of ionization at pH 2 to 4, but under the conditions of pH 6 to 8, it is possible to see a greater difference in both indicators. The simulation results show that the degree of ionization begins to decrease at approximately pH 5 or 6, but the ζ-potential begins to decrease at lower pH conditions.

Silica, on the other hand, has a greater variation in the degree of ionization under relatively low pH conditions, unlike alumina. The simulation results show a greater variation in the degree of ionization from about pH 3 or 4, and little change at pH 7 to 8. The experimental results show that the ζ-potential changes greatly from pH 0.5. However, the variation in the ζ-potential under pH 6 to 8 was not significant, as was the degree of ion-

ization difference in the simulation results. Therefore, we could not compare the same physical value exactly, but we could obtain a titration curve for the alumina and silica groups with a trend similar to the experimental results.

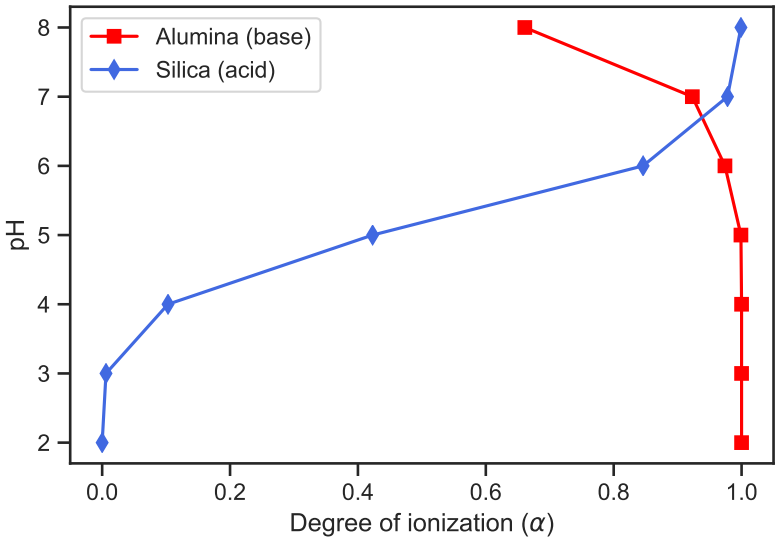

Figure 4.3: Titration curve of degree of ionization from alumina and silica on simulated HNT surfaces.

So far, we have seen how many surface groups have been charged and it can be explained by the definition of acid-base theory by Lewis, that is,

> Basic substance has a lone pair of electrons which may be used to complete the stable group of another atom, and that an acid substance is one which can employ a lone pair from another molecule [56].

Here, alumina can be explained as a basic substance, and silica can be explained as an acidic substance. Therefore, figure 4.1 is replotted into figure 4.3 as the pH is placed on the y-axis and α without sign is placed on the x-axis for comparing with the titration curves of acid and base in figure 4.4.

The x-axis in figure 4.4 corresponds to the amount of added acid/base from result of the experiment [57]. Thus, each physical value on the x-axis in figure 4.4 and figure 4.3 are not exactly the same physical values, but the two results were compared under the

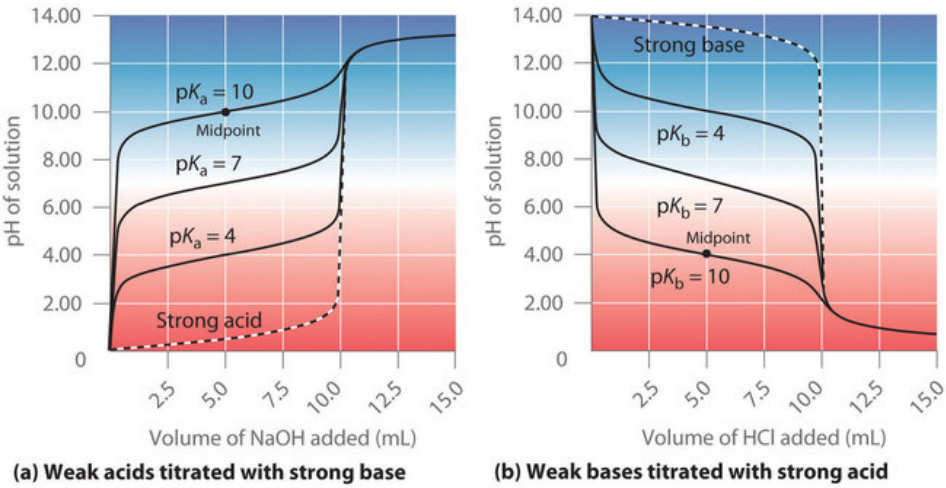

Figure 4.4: Titration curve of (a) acid regarding different pK_a values and (b) base with different pK_b value. Note that, in aqueous solution at 298 K, pK_a + pK_b = 14 [54]. Image is adaped from [55]

assumption that they would indicate how many charged particles in the system (including the surface groups present at fixed position).

We can see a blue titration curve in figure 4.3 and curves of weak acids in figure 4.4 (a) have similarities in there shapes. Meanwhile, pH value of inflection points from titration curves in figure 4.4 (a) notifys pK_a of each curve. We can see the inflection point of the curve in figure 4.3 is slightly shifted (pH of inflection point is supposed to be 4.23 but about 5).

This is regarded as a shift because of an influence of neighboring surface groups. HNT is made of surface groups and there are dissociation sites on the surfaces, unlike a monoprotic acid which has a dissociation site that donates only one proton. In other words, HNT is more difficult to be ionized than a monoprotic acid even if they are in same pHcondition. This is because from the perspective of one specific surface group, if the surface groups around it are already ionized, the ionization is unfavorable. This is in the same vein as the reason why a weak PE has difficulty in dissociating monomers which have neighboring ionized monomers in a chain referred from Stornes and co-workers [58].

Furthermore, titration curves of the HNT in the presence of a negatively charged and a positively charged PE were compared as shown in figure 4.5. Three curves of the outer

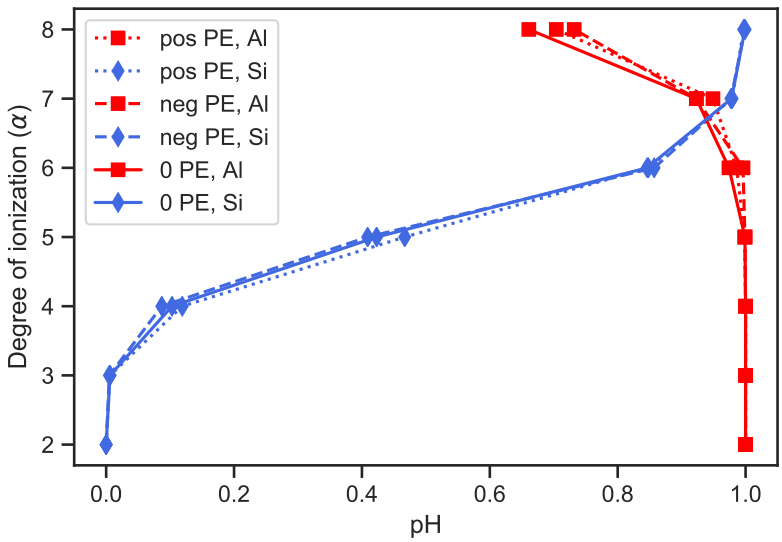

Figure 4.5: Titration curve of three different systems.

surface (silica, diamond marker) of a HNT show very similar titration behaviors with the exception of systems at pH 4 and 5 regardless of the presence of a negatively/positively charged PE, or the absence of the HNT.

Three curves of the inner surface (alumina, square marker) of the HNT also show very similar behaviors except systems of pH 6, 7 and 8. That is, the degree of ionization of alumina and silica depends on pH, but are not much affected by the presence and the negativity/positivity of the PE has.

In this study, in particular, when designing a model of how the ionization process is carried out (how pK_a affects the protonation and deprotonation in simulations), a method (constant-pH ensemble method) that mimics the natural aqueous solution was used as an alternative, as described in sec:methods. The above results are the basis for determining the applicability of this method in a perspective of pH-dependent behavior.

4.2 Polyelectrolyte behavior

Here, one single PE which is positively or negatively charged, and a HNT are studied under different pH conditions from 2 to 8. Focus is given to the conformational characteristics of the PE, which are (1) R_g, (2) R_{ee}, and the adsorption behavior of the PE through indicators such as (3) number of adsorbed segments, (4) loops, tails, and trains analysis, and (5) contact probabilities.

4.2.1 Conformational characteristics

Radius of gyration

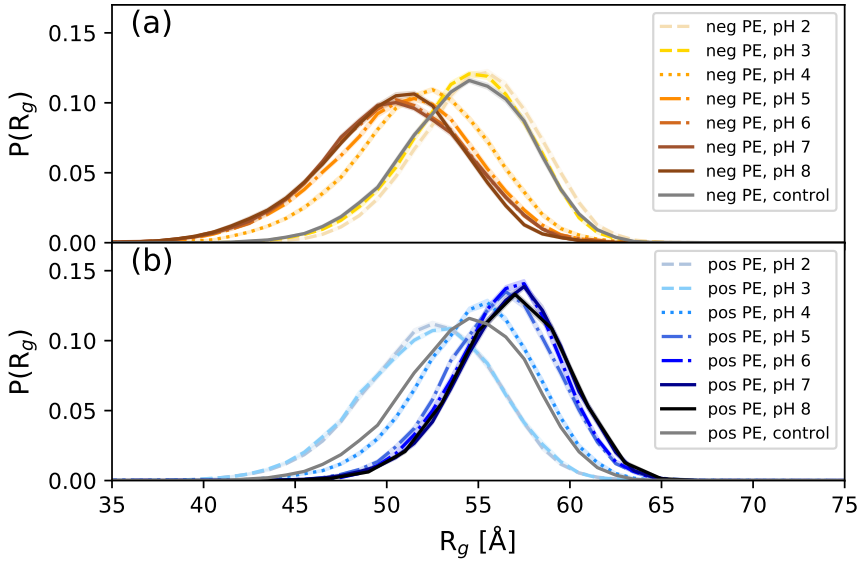

Figure 4.6: Probability distribution of R_g at increasing pH, with a negatively charged (a) and positively charged (b) PE. Colors become darker at increasing pH ranging from 2 to 8. The control group, PE without a HNT is shown with the gray line. Errors (standard deviations) of each line are shown as shadowed regions in the same colors as the corresponding lines, with about the same thickness of the lines.

We have evaluated the probability distribution functions of R_g for the positive and negatively charged PEs in the presence of HNT, shown in figure 4.6 (a) and (b). It can

be seen that the R_g distribution shifts at increasing pH (as blue colors of lines and orange colors of lines become darker). Starting with a negatively charged PE, it is shown that the distribution at pH 2 (yellow and dashed line) has its highest probability at about 54.8Å in figure 4.6 (a). The distribution shifts towards smaller R_g value as pH increases. The $P(R_g)$ of the PE at pH 2 and 3 (dashed lines) nearly overlap with that of the control group, but the size distribution for pH 4 (dotted line) is shifted to smaller sizes, and further more for the size of pH from 5 to 8 (dash-dotted and solid lines) are seen as having similar feature. There is a decreasing trend of R_g as pH increases

On the other hand, it can be seen in figure 4.6 (b) that the distribution of a positively charged PE at pH 8 (dark blue and solid line) shows a maximum at around 56.7Å, and the distribution shifts towards higher R_g value with increasing pH. Among different pH conditions, a positively charged PE tends to show similar size, distribution at pH 2 and 3 (dashed lines) and above pH 5 (dash-dotted and solid lines).

Consequently, the probability distribution of R_g shows a different trend from the positive and negatively charged PEs at increasing pH, but both show a significant conformational change in the pH interval of from 3 to 5.

End-to-end distance

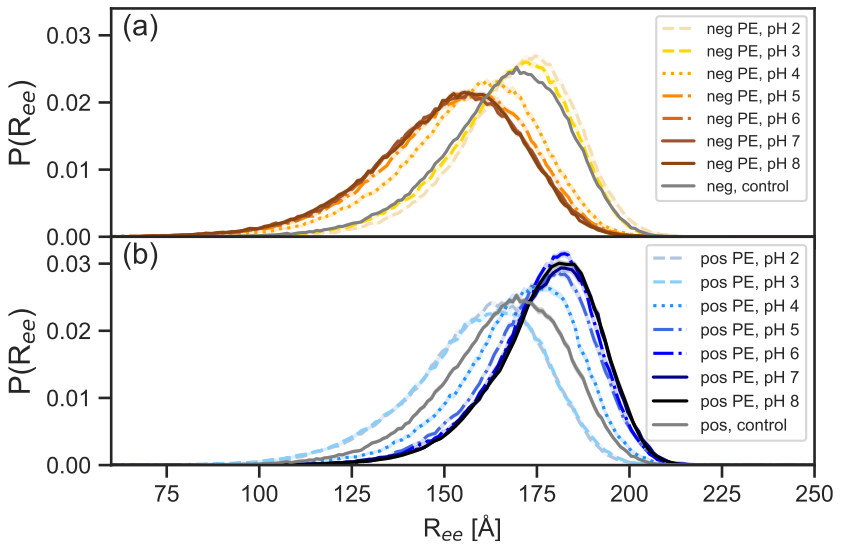

Figure 4.7: probability distribution of the end-to-end distance (R_{ee}) of one PE, negatively charged (a) and positively charged (b) at increasing pH. Colors become darker at increasing pH ranging from 2 to 8. The control group, PE without a HNT is shown with the gray line.

The probability distribution functions of R_{ee} in figure 4.7 (a) and (b) show the same overall behaviors than that shown for $P(R_g)$ to one of R_g in figure 4.6. The distributions of R_{ee} tend to be more asymmetric than them of $P(R_g)$, but similar trends were observed with pH variations. With the $\left\langle R^2 ee \right\rangle^{1/2}$ varying from 169.3 Å to 150.3 Å when pH varies from 8 to 2 for a negatively charge PE, and for the positively charged PE varying from 158.6 Å to 177.5 Å with pH from 2 to 8. In short, R_{ee} shows a different trend from the positive and negatively charged PE, like R_g.

4.2.2 Adsorption and contact analysis

Number of adsorbed segments and chains

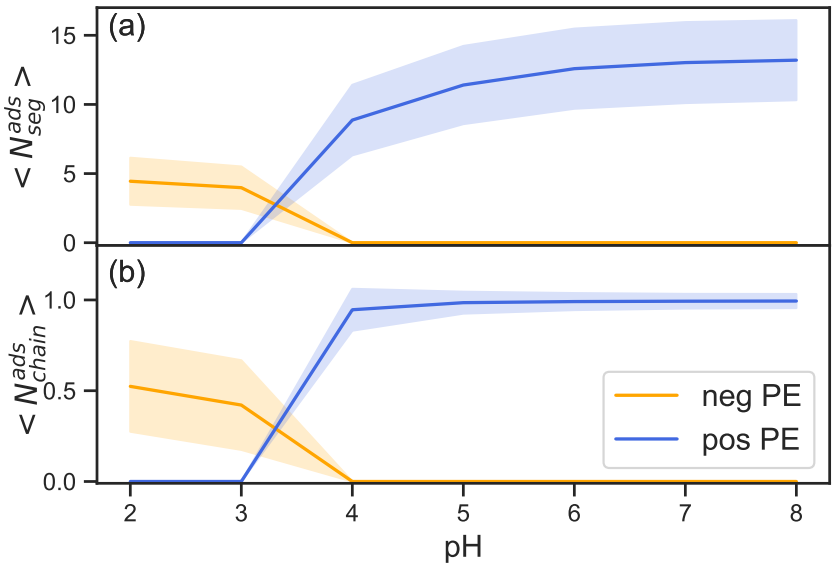

Figure 4.8: The averaged number of and adsorbed segments ($\langle N_{\text{seg}}^{\text{ads}} \rangle$) (a) and adsorbed chains ($\langle N_{\text{chain}}^{\text{ads}} \rangle$) This a system of only one PE so the maximum number of $\langle N_{\text{chain}}^{\text{ads}} \rangle$ is 1.

Figure 4.8 shows the average number of adsorbed segments ($\langle N_{\text{seg}}^{\text{ads}} \rangle$ in (a)) and the average number of adsorbed chains ($\langle N_{\text{chain}}^{\text{ads}} \rangle$ in (b)). $\langle N_{\text{seg}}^{\text{ads}} \rangle$ increases as pH increases above 3 for the positively charged PE (blue line), and it reaches a plateau region. $\langle N_{\text{chain}}^{\text{ads}} \rangle$ sharply goes up as pH changes from 3 to 4, and it does not vary above pH 4, that is an available maximum number of chains in this system, one. The result of $\langle N_{\text{chain}}^{\text{ads}} \rangle$ is coherent with that of $\langle N_{\text{seg}}^{\text{ads}} \rangle$, considering a chain is regarded as an 'adsorbed chain' when there is one or more segments adsorbed.

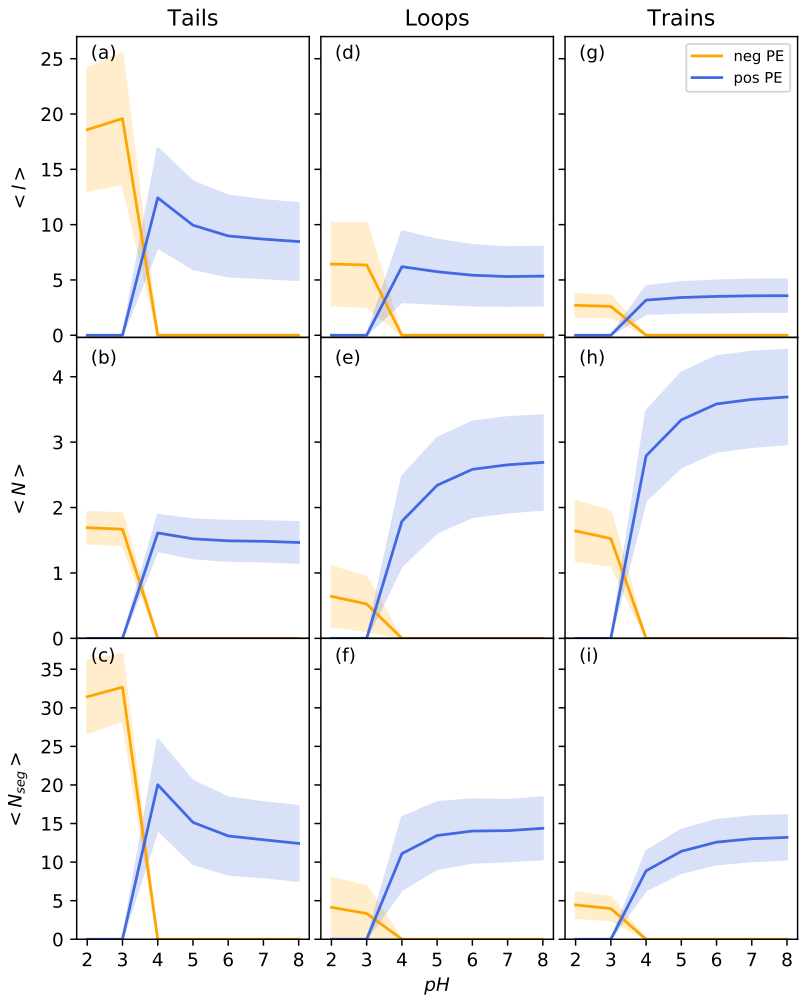

Figure 4.9: Loops, tails, and trains analysis of a negatively charged and positively charged PE at increasing pH. Units in Å or real number. Errors (standard deviations) of each lines are shown as shadowed regions in the same colors as the corresponding lines.

In contrast, $\left\langle N_{\text{seg}}^{\text{ads}} \right\rangle$ and $\left\langle N_{\text{chain}}^{\text{ads}} \right\rangle$ of a negatively charged chain are zero at pH values above 3. figure 4.8 (a) shows a moderate number of monomers of the negatively charged

PE adsorbed to the HNT with only up to 5 segments for pH values of 2 and 3; above it, the PE does not adsorb (orange line). This is a coherent with result of panel (b) which shows $\left\langle N_{\text{chain}}^{\text{ads}} \right\rangle$, and indicates that at pH values of 2 and 3 the chain is adsorbed to the HNT about half of total configurations while if drops to zero for pH 4 and above.

Loops, tails and trains analysis

Three indicators, the average length ($\langle l \rangle$ [Å]) per one element, the average number of the elements ($\langle N \rangle$) and the average number of segments ($\left\langle N_{\text{seg}} \right\rangle$) of the elements, were evaluated for each of three PE structural elements, loop, tail and train. Thus, indicators are $\left\langle l^{\text{loops}} \right\rangle$, $\left\langle l^{\text{tails}} \right\rangle$, $\left\langle l^{\text{trains}} \right\rangle$, $\left\langle N^{\text{loops}} \right\rangle$, $\left\langle N^{\text{tails}} \right\rangle$, $\left\langle N^{\text{trains}} \right\rangle$, $\left\langle N_{\text{seg}}^{\text{loops}} \right\rangle$, $\left\langle N_{\text{seg}}^{\text{tails}} \right\rangle$ and $\left\langle N_{\text{seg}}^{\text{trains}} \right\rangle$, all shown in figure 4.9. These indicators are mutually related to each other, for example, the number of loops is equal to (the number of trains - 1) since loops are formed between two trains. This is shown as $\left\langle N^{\text{loops}} \right\rangle$ and $\left\langle N^{\text{trains}} \right\rangle$ in (e) and (h). Under pH condition where the chain does not adsorb, these indicators will be zero, which occurs for the negatively charged PE above pH 3 and positively charged PE below pH 4.

For a positively charged PE (blue lines), $\left\langle N^{\text{trains}} \right\rangle$ (h) and $\left\langle N^{\text{loops}} \right\rangle$ (e), $\left\langle N_{\text{seg}}^{\text{trains}} \right\rangle$ (i) and $\left\langle N_{\text{seg}}^{\text{loops}} \right\rangle$ (f) increase and reach a plateau region as pH increases. $\left\langle l^{\text{tails}} \right\rangle$ (a) and $\left\langle N_{\text{tails}}^{\text{seg}} \right\rangle$ (c) decrease from pH 4 and reach plateau at increasing pH. This indicates that the number of loops and trains grow at the expense of tail monomers, consistent with a stronger PE adsorption as pH increases. $\left\langle l^{\text{loops}} \right\rangle$ (d) and $\left\langle l^{\text{trains}} \right\rangle$ (g) are nearly constant above pH 3.

Meanwhile, the adsorption of the positively charged PE on the surface starts, for pH 4, $\left\langle N^{\text{loops}} \right\rangle$ (e), $\left\langle N_{\text{seg}}^{\text{loops}} \right\rangle$ (f), $\left\langle N^{\text{trains}} \right\rangle$ (h) and $\left\langle N_{\text{seg}}^{\text{trains}} \right\rangle$ (i) increase as pH increases but the length of loops and trains do not ($l\left\langle^{\text{loops}}\right\rangle$ (d) and $l^{\langle \text{tails} \rangle}$ (a)). We can infer that even though the conditions lead to an increase in adsorption of the PE in terms of the total number of adsorbed segments and trains onto the surface, the length of each train does not increase. This may be due to the fact that the surface of the HNT is not homogeneous but made of discrete surface groups. The distance between neighbored surface groups or the size of the CG bead of surface group may concern the unchanged $\left\langle l^{\text{loops}} \right\rangle$ (d) and l^{tails} (a). In order to improve the simulation, further work should be conducted using a smaller CG bead or shorter bead-bead distance to mimick the continuous surface.

The negatively charged PE only shows adsorption at pH 2 and 3, so it is challenging to confirm trends of the indicators of interest as pH condition changes (see orange lines in

figure 4.9). However, the formation of long tails is more dominant than loops and trains when compared to the positively charged PE. This can be found from the relatively large $\langle l^{\text{tails}} \rangle$ (a) and $\langle N_{\text{seg}}^{\text{tails}} \rangle$ (c), and small $\langle l^{\text{loops}} \rangle$ (d), $\langle N_{\text{seg}}^{\text{loops}} \rangle$ (f), $\langle l^{\text{trains}} \rangle$ (g) and $\langle N_{\text{seg}}^{\text{trains}} \rangle$ (i).

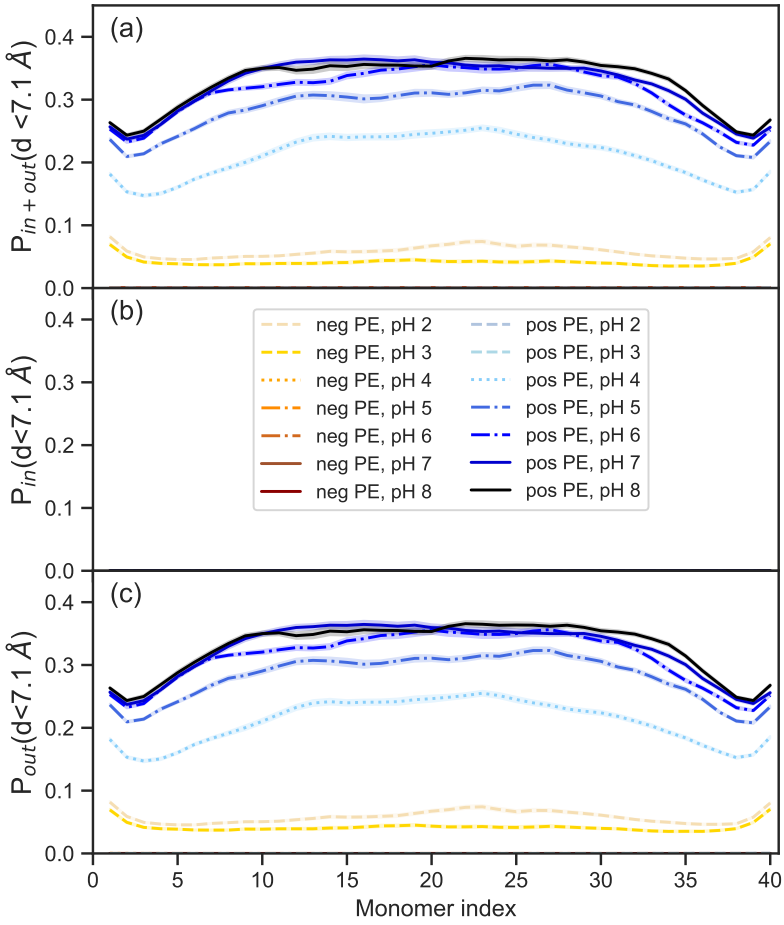

Figure 4.10: Contact probability distribution of a PE. Colors become darker as pH increases from 2 to 8. Adsorption on the inner surface of the tube (b), the outer surface (c), and both surfaces (a).

Contact probabilities onto surfaces

Here the adsorption behavior of the PE is discussed by evaluating the contact probabilities of the individual monomers. Starting with the positively charged chain, monomers are adsorbed on the outer surface of the tube at pH conditions above 3, as shown by the blue dotted and solid lines in figure 4.10 (c). It can be seen that the probability of finding adsorbed monomers increases with the pH, in good agreement with $\left\langle N_{\text{chain}}^{\text{ads}} \right\rangle$ and $\left\langle N_{\text{seg}}^{\text{ads}} \right\rangle$ in figure 4.8. Figure 4.10 also shows that the central monomers of the PE have roughly the same probability of adsorption but this decreases when moving forward the ends, to increase again at the end monomers. This gives rise to a distribution with two minima close to the ends, but not at the ends. The shape of contact analyses is monotonous along the chain except two ends.

Interestingly, a negatively charged PE shows adsorbed monomers on the outer surface of the HNT at low pH (see yellow and dashed lines in figure 4.10 (c)). The contact probability is not very large, which accounts for the small number of adsorbed segments with only up to 5 segments for pH value of 2 and 3 (figure 4.8 (a)). Above pH 5, the PE does not adsorb (orange line). Surprisingly, the negatively charged PE shows no adsorption to the inner surface, even though the degree of ionization of alumina is 1.0 (all alumina groups are positively charged) as previously discussed, regarding to titration curves shown in figure 4.1.

Due to the lack of adsorption to the inner surface, the contact probability of both inner and outer surfaces is equal to that of the adsorption on the outer surface. The shape of contact analyses shows a convex curve, which is different from the curve with the double minima seen from the positively charged chain (blue line)

4.3 Discussion

Dependence of R_g with pH

The averaged R_g of the negatively charged PE decreases as pH increases, and the opposite occurs with a positively charged PE. A pH increase or decrease affects α of surface groups as it was discussed previously, as well as α of charged counter ions of the corresponding surface groups. Therefore, we can discuss that has the variation of R_g under different pH conditions can be caused by two reasons: (1) self-screening effect due to the presence of the HNT, and (2) conformational change due to adsorption to surface.

The strongly charged PE loses its counterions, and monomers in the chain feel a repulsive Coulombic force in salt-free solution. Existence of added co-ions reduces the Coulombic repulsion, so called *screening effect*. The screening is ensured by free ions which have high mobility and include not only added salt ions but also counterions which are present due to electroneutrality of the system [59, 60, 61].

To compare a screening effect from a variation of pH, the α of surface groups of the HNT is utilized for assessing the number of charged ions in each system. There are three types of counterions in each system. (1) Counterions of alumina groups on the inner surface, (2) counterions of silica groups on the outer surface, and (3) counterions of the PE. Each counterion group has a number of 100, 500 and 40 particles respectively. α of each conditions and total charge (Q_{tot}) resulting from counterions can be calculated by α referred from the titration curves in figure 4.3. When calculating Q_{tot}, we use an intuitive and simple equation which is given by

$$Q_{\text{tot}} = -\alpha_{\text{al-ci}} \cdot n_{\text{al-ci}} + \alpha_{\text{si-ci}} \cdot n_{\text{al-ci}} \pm \alpha_{\text{pe-ci}} \cdot n_{\text{pe-ci}} \tag{4.1}$$

$$= -100\alpha_{al} + 500\alpha_{si} \pm 40\alpha_{pe} \tag{4.2}$$

where α the is degree of ionization of charged particles and n is number of particles available in the system. Note that a sign of ± depends on whether a PE is negatively or positively charged. These are listed specifically in table 4.1.

Table 4.1: List of indicators for evaluating R_g trends of PEs. $\alpha_{\text{pe-ci}}$ is α of PE counterion, $\alpha_{\text{al-ci}}$ for counterion of alumina groups and $\alpha_{\text{si-ci}}$ for counterion of silica groups. Q_{tot} is the total charge of charge from all mobile ions in a system. Control means a system of a PE without HNT (a).

PE type	pH	$\left\langle R_g^2 \right\rangle^{1/2}$ [Å]	$\alpha_{\text{pe-ci}}$	$\alpha_{\text{al-ci}}$	$\alpha_{\text{si-ci}}$	Q_{tot}
Negatively charged PE	2	54.9	1	1	0	-60
	3	54.3	1	1	0.005	-57.5
	4	51.8	1	1	0.087	-16.5
	5	51.7	1	0.999	0.409	145
	6	50.4	1	0.996	0.857	369
	7	50.3	1	0.923	0.977	436
	8	50.2	1	0.732	0.999	466
	Control[a]	54.2	1	0	0	40
Positively charged PE	2	52.3	1	1	0	-140
	3	52.2	1	1	0.006	-137
	4	54.8	1	1	0.119	-80.5
	5	56.2	1	0.999	0.467	93.6
	6	56.5	1	0.986	0.848	285.4
	7	56.7	1	0.949	0.979	354.6
	8	56.8	1	0.704	0.997	388.1
	Control[a]	54.0	1	0	0	-40

For a positively charged PE, the repulsive force between monomers is partially cancelled out by free anions, and the degree is determined by the negativity of Q_{tot}. At pH 2, anions dominantly exist in the system and monomers are screened by electrostatic force from anions and the chain tends to condense (R_g decreases). On the other hand, cations are dominant in a system of pH 8 and the chain is more extended than the chain at lower pH condition. Q_{tot} of the control is higher than Q_{tot} at pH 4 and lower than Q_{tot} of pH 5 while the R_g of the control shows an average R_g is with in the range of R_g of pH 3 and 4.

A negatively charged PE condenses more at pH 8 than pH 2 in the result of abundant cations with Q_{tot} of 466 at pH 8 where the screening effect is maximized (see table 4.1). However, for both PEs, it is not explained that R_g of the control group is between two

values, R_g of pH 3 and R_g of pH 4. Moreover, for a negatively charged chain, the size distribution of the control PE nearly overlap with the distribution of the PE in the presence of the HNT at pH 2 or 3.

In other words, the screening effect can explain trends of R_g of negatively and positively charged PE, in the opposite directions. However, it can not explain that why the size of R_g of the control shows an average within the range of R_g of pH 2 and 3 for the negatively charge PE. We consider the other factor here, that is, change of conformation due to adsorption onto the tube by reminding the fact the negatively charge PE shows an adsorption at pH 2 and 3 in figure 4.8 and 4.10. The adsorption may make the PE extend or condense but we can not conclude yet.It should able to explain a extension of a positively charged PE at pH 8, however, we can not judge that an increase of R_g at pH 8 is due to only screening effect, or both.

In order to prove (1) the effect of counter ions and (2) an extension or condensation by adsorption, further simulations are suggested. To verify the effect of counterions, it is suggested an evaluation of R_g by comparing two systems, which are a system of a PE and a HNT with alumina only, or only silica. Then we can compare the conformational variation that results from the number and α of counterions, respectively.

To verify the relationship between R_g and the adsorption characteristic, variation of size of the tube or curvature of the outer surface, and the ratio of external radius of the tube to length of PE can be considered. These are examples of studying spacial exclusion of a PE. This verification is important. It is recalled that a PE here represents an enzyme, a protein, and the goal of this study is to find HNT as the potential for stabilizing and carrying it. Thus, the characteristics associated with adsorption and the variation of conformation due to adsorption need to be studied together with other factors that cause the change in conformation.

Contact probability and adsorption

Surprisingly, the contact probabilities show that the negatively charged PE adsorbed on the outer surface and not the inner surface, as expected.

A conformation where a negatively charged PE adsorbs out the positively charged surface groups on the inner surface of the tube, was expected to be that the most stable state, that is, an equilibrium state, but the results from the simulated system shows our

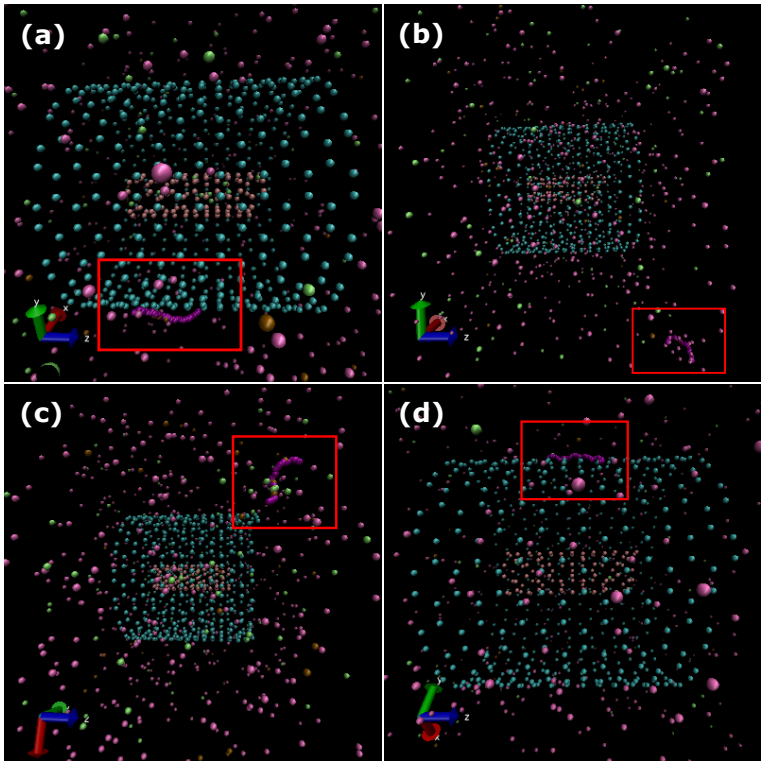

Figure 4.11: Representative snapshots of (a) negatively charged PE at pH 2 and (b) pH 8, and positively charged one at pH 2 (c) and pH 8 (d). The PE is depicted as a chain with deep purple color in a red box.

expectation was wrong. Even though a repulsive interaction with the outer surface (silica) can be neglected since the groups on the outer surface have no fractional charge at pH 2, the negatively charged PE is not found to occupy the inside the HNT (lumen), as shown in snapshots of figure 4.3.

To make it easier to understand what is described above, let us look at a electrostatic potential energy. By calculating the energy whether it is inside or outside the tube, it should be possible to see what would be the preferential location of the PE.

Figure 4.3 shows the simplified scheme. It assumes that a location of a PE and the center of the tube both are projected on the horizontal plane (*i.e.* $z = 0$), and the distance between them is redrawn on the linear axis by the fact that HNT is cylidrically symmetric. The location of the PE is described as a green dot, on the axis. This approximation is based

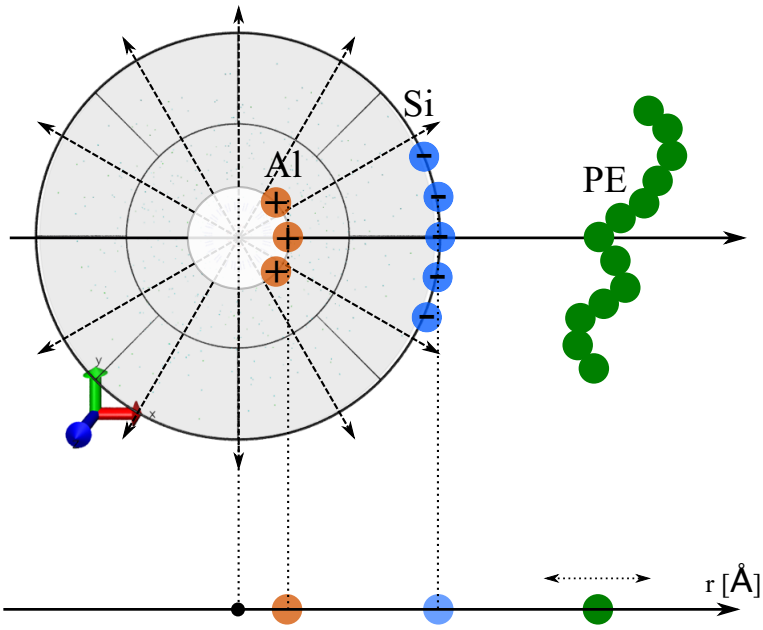

Figure 4.12: Schematic illustration of HNT by horizontal view. Alumina (orange) and silica (blue) surface groups are shown on the radial axis from the central axis of the tube. A green dot is a location of a PE and a black dot is the center of the tube. U_{el} is calculated by a distance between two point charges instead of a charge and a surface.

on the assumption that the surface charge density of the tube is constant, and all points on this surface are equally charged on a macroscopic scale, and this point represented as a orange and blue dots. In addition, this approach does not take into account the electrostatic interaction of simple ions (counterions) with the surface groups or PE. Thus, although the results obtained from this approximation cannot give the exact equal value of system's $U_{nonbond}$ in equation 3.2, we can roughly estimate the energy and stability of the system according to the location of the PE.

Based on the approximations explained above and in figure 4.3, the estimated electrostatic potential energy, U_{el}, of a simple system composed of beads of alumina, silica, and PE (positive/negative), except counter ions, is calculated according to [62],

$$U_{\mathrm{el}} = \frac{1}{4\pi\epsilon_0}\frac{q_{al,i}q_j}{|60-r|} + \frac{1}{4\pi\epsilon_0}\frac{q_{al,i}q_j}{|60+r|} + \frac{1}{4\pi\epsilon_0}\frac{q_{si,i}q_j}{|300-r|} + \frac{1}{4\pi\epsilon_0}\frac{q_{si,i}q_j}{|300+r|} \tag{4.3}$$

where r is a distance from the center of the tube lumen as indicated in 4.3, q_j is the charge of monomer in the chain, $q_{al,i}$ is the average charge of alumina at pH i, and $q_{si,i}$ for silica, which are estimated by α.

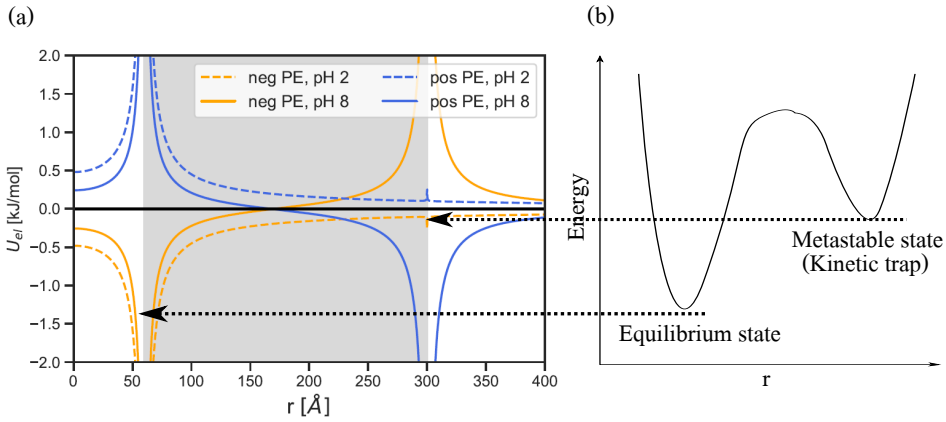

Figure 4.13: (a) Electrostatic potential energy of the system, as a function of the distance measured from the center of a tube on the horizontal plane. The gray area, $60 < r < 300$, indicates the wall of the HNT. (b) Schematic energy diagram of a kinetic trap.

The electrostatic potential energy, U_{el}, calculated according to equation 4.3 is plotted in figure 4.13 (a). The negatively charged chain located in the outer area of a tube at a radial distance $r = 307.1$Å has negative U_{el} at pH 2 condition. Therefore, an adsorption of a PE onto the outer surface is natural.

However, as expected, U_{el} is more negative for the tube lumen than the outer area. By looking at this from the perspective of the Metropolis algorithm and the energy of this system, we can infer that the configurations where the chain exists in the lumen has sufficiently low energy to justify a large number configurations, in other words, it is a stable state. Although the total energy of the system may be lower with the chain inside the tube, intermediate moves can be rejected if trial moves for changing configuration of the chain into the lumen can have a much higher energy than the previous step.

As such, the system does not appear to have reached the global minimum but has reached a local minimum. Although it is not the most stable state thermodynamically, but it is the relatively stable state which is called *metastable state* [57]. If this concept is applied to the system described earlier, we can assume that (1) the chain is inside as an

equilibrium state, and that (2) the chain is stably adsorbed onto the outer surface of the tube, as a metastable state. This is described in figure 4.13 (b). If this assumption is true, it can be expected that the system will reach the equilibrium state when more trial moves are carried out. However, it is not known how long simulation will be needed in this case.

We carried out 40 more macrosteps, so total $60 \cdot 20,000$ steps, but the negatively charged PE did not go into the lumen. Therefore, we implemented an equilibrium run for the system with a PE generated in the lumen.

4.4 Polyelectrolyte generated in tube lumen

As mentioned, a set of simulations was performed where the PE is generated in the lumen of the tube. The reason was two-folded: Firstly, to study adsorption behavior of the PE in the HNT lumen. Secondly, to assess the difference in energy between the two states (inner and outer adsorption) and proving that a PE is more stable when inside. If the assumption that 'The negative PE adsorbs to the external surface at low pH values due to a kinetic trap.' is correct, the energy of the system should be lower when the PE is inside the tube, than when it absorbs to the outer surface.

Indeed, considering the obtained energy values, it can be concluded the system where the PE occupies the center of the HNT as a lower total energy (0.157 ± 0.008 kJ/mol) than the systems where the PE is randomly generated and adsorbs on the surfaces (0.259 ± 0.019 kJ/mol).

4.4.1 Contact analysis

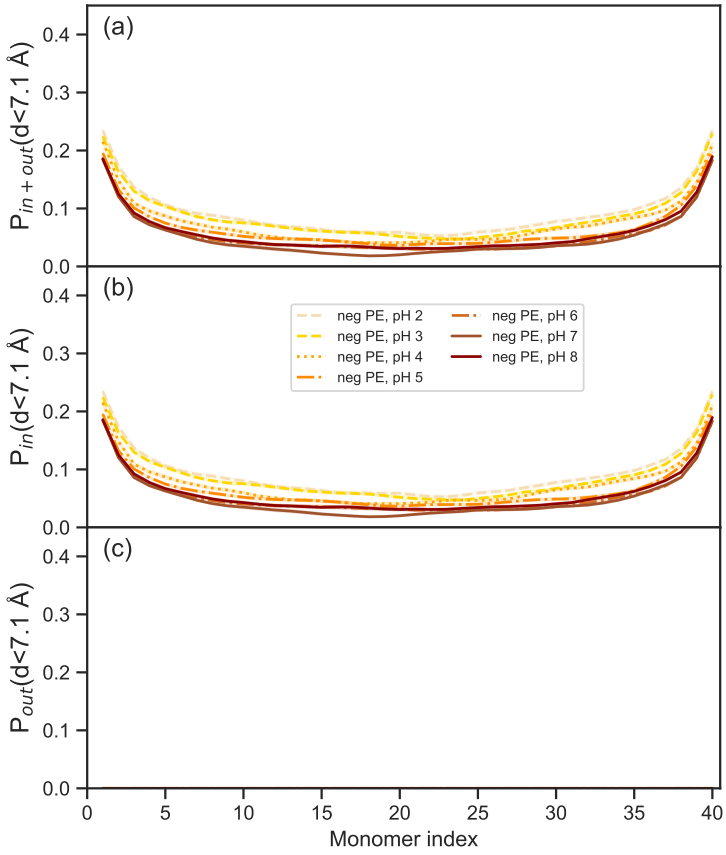

Figure 4.14: Contact probability distribution of a PE generated in the lumen. Colors become darker as pH increases from 2 to 8. Adsorption on the inner surface of the tube (b), the outer surface (c), and both surfaces (a).

Therefore, we can conclude that the reason a PE adsorbs onto the outer surface at pH 2 is because it gets caught on a kinetic trap.

Contact analysis in figure 4.14 shows a different profile than that discussed in fig-

ure 4.10. Firstly, it shows contact probabilities different than zero for monomers at all studied pH conditions at the inner surface, not the outer surface. In particular, contact probabilities increase as pH decreases from 5 to 2, which is a number of charged alumina on the inner surface increases in this pH range. Above this pH the curves mostly overlap.

4.4.2 Density distribution

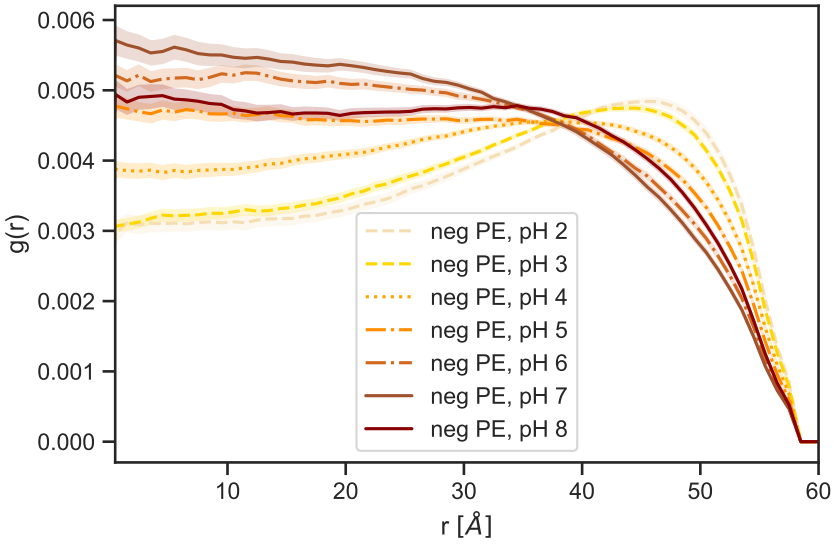

Figure 4.15: Radial density projectedraid on the $z = 0$ plane. Colors become darker as pH increases from 2 to 8. Errors (standard deviations) of each lines are shown as shadowed regions in the same colors as the corresponding lines.

The radial density projected on the $z = 0$ plane is shown in figure 4.15. At low pH there is a clear maxima close to the inner wall of the HNT, with a peak at around $r = 47$Å. Note that this maximum is outside the adsorption threshold, 7.1 Å. As the pH increases, the maximum becomes less pronounced from a pH of 5 and above the PE monomers are found with a constant density in the center of the lumen and their presence decays forwards the inner wall of the HNT. This is in good agreement with the decrease in the number of adsorbed monomers seen in figure 4.14. The point which has a peak in each distribution shifts left (r value decreases) as pH value varies from 2 to 5, the distribution of pH 7 has the

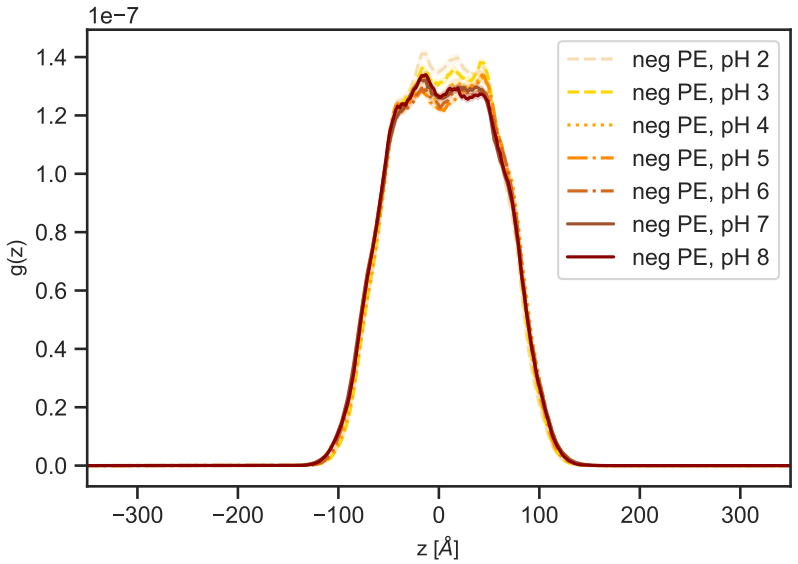

Figure 4.16: Number density in the z-direction.

highest value of probability at $r = 0$Å, the exact central axis of the tube. The distribution at pH 2, 3, and 4 shows an inflection point, but the distribution transforms to a concave curve as pH increases.

Figure 4.16 shows the number (monomer) density along the z coordinate, that is, the monomer occupancy along the HNT. As it can be seen the plots are very similar for the different pH values. The PE tends to occupy the central part of the HNT and rarely exists at $z < -100$Å or $z > 100$Å.

Taking figure 4.15 and 4.16 together, we can deduce that a negatively charged chain within the lumen of the HNTs, not outside of the HNT gives rise to conformations with lower energy, as expected. It can be seen a variation in pH affects the conformation of PE, especially radial distribution. At low pH condition, PE occupies a position due to the inner surface of the tube, but as the pH increases the occupance by the inner surface decreases. This can be due to the repulsive interactions with the silica groups on the outer surface.

4.5 Statistical analysis

So far, we have studied only one structure of PE with architecture of all 40 monomers which are negatively or positively charged. The intention was to study how a PE interacted and behaves with the HNT without considering specific structural characteristics of the PE. From here, we evaluate how the PE architecture variable correlates with the conformation of PE by analysis of the ensemble average of radius of gyration ($\left\langle R_g^2 \right\rangle^{1/2}$) and number of adsorbed segments on the inner surface and outer surface ($\left\langle N_{\text{seg}}^{\text{ads,in}} \right\rangle$ and $\left\langle N_{\text{seg}}^{\text{ads,out}} \right\rangle$).

4.5.1 Ensemble-averaged radius of gyration

Correlation analysis

Table 4.2: Table of Spearman's correlation coefficient (r) of $\left\langle R_g^2 \right\rangle^{1/2}$ with each variable. Strength of relationship with p-value is also given.

Variables	r	Strength	p-value
N_{block}	-0.565	Moderate	0.000
$\lvert Z_{\text{net}} \rvert$	0.890	Very strong	0.000
R_{core}	0.603	Strong	0.000
N_{mon}	0.473	Moderate	0.000
Z_{net}	-0.302	Weak	0.001
pH	0.087	Very weak	0.348

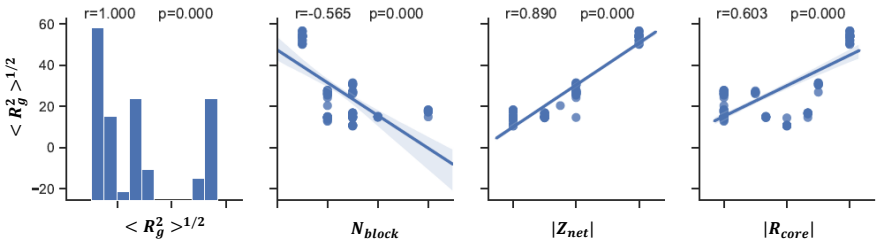

Figure 4.17: Multi-dimensional scattering plot of $\left\langle R_g^2 \right\rangle^{1/2}$ and three variables; N_{block}, $|Z_{net}|$, and R_{core}. These are variables which show correlation coefficients higher than 0.5 ($r > 0.5$) with $\left\langle R_g^2 \right\rangle^{1/2}$. Coefficients are displayed with p-values.

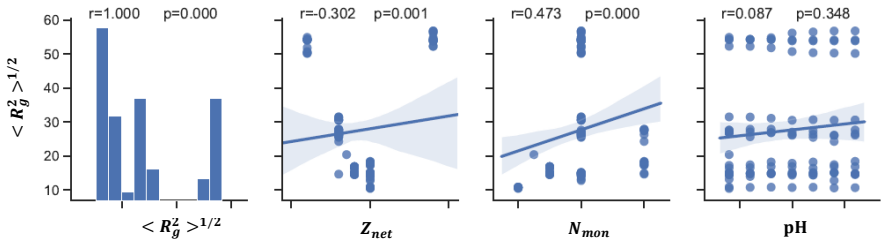

Figure 4.18: Multi-dimensional scattering plot of $\left\langle R_g^2 \right\rangle^{1/2}$ and three variables; Z_{net}, N_{mon}, and R_{core}. These are variables which show correlation coefficients less than 0.5 ($r < 0.5$) with $\left\langle R_g^2 \right\rangle^{1/2}$. Coefficients are displayed with p-values.

In figure 4.17, particularly $\left\langle R_g^2 \right\rangle^{1/2}$ increases as $|Z_{\text{net}}|$ increases with few points to drop or jump suddenly, which violates a monotonous increase. This is with good agreement of high r in table 4.2 as a strong correlation with $r = 0.89 \geq 0.8$. Therefore, $|Z_{\text{net}}|$ is more strongly correlated with the size of R_g than any other variables.

In contrast, the scatter plot of pH shows a repetitive pattern of $\left\langle R_g^2 \right\rangle^{1/2}$ as pH increases, that is coherent with high p-value ($0.348 > 0.05$) in table 4.2, which states pH is not significantly correlated with $\left\langle R_g^2 \right\rangle^{1/2}$ with a 95% confidence. This is interesting because a variation of R_g is shown as pH varies in figure 4.6. The size of R_g is dependent on a variation of pH when a PE is homogeneously charged, but the correlation is not significantly strong as much as other factors (variables) when the PE is non-homogeneous.

Meanwhile, regarding the sign of r values, N_{block} and Z_{net} have a negative correlation to $\left\langle R_g^2 \right\rangle^{1/2}$, however, all variables except these have a positive correlation to $\left\langle R_g^2 \right\rangle^{1/2}$.

To sum up, variables have higher correlation association to $\left\langle R_g^2 \right\rangle^{1/2}$ in order of $|Z_{\text{net}}| > R_{\text{core}} > N_{\text{block}} > N_{\text{mon}} > Z_{\text{net}} >$ pH, and only N_{block} and Z_{net} have a negative correlation with $\left\langle R_g^2 \right\rangle^{1/2}$.

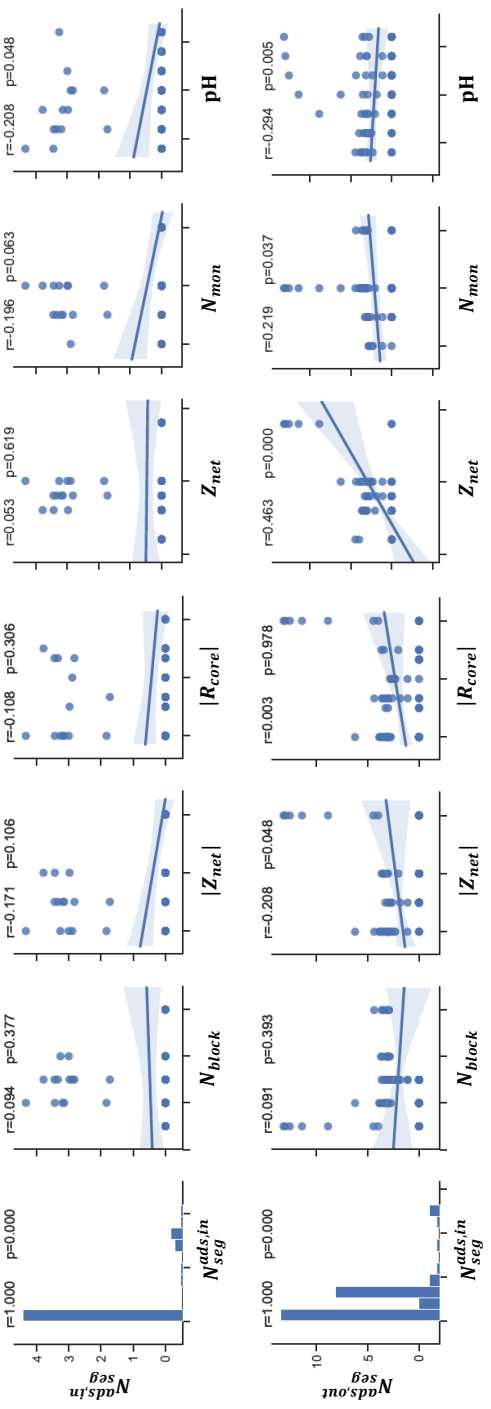

Figure 4.19: Multi-dimensional scattering plot of number of adsorbed segments onto inner surface and outer surface ($N_{seg}^{ads,in}$ and $N_{seg}^{ads,out}$) with six variables ;$|Z_{net}|$, R_{core}, N_{block}, N_{mon}, Z_{net}, and pH

4.5.2 Number of adsorbed segments

Correlation analysis

Table 4.3: Table of Spearman's correlation coefficient (r) of $N_{seg}^{ads,in}$ and $N_{seg}^{ads,out}$ with each variable. Strength of relationship with p-value is also given.

	$N_{seg}^{ads,in}$			$N_{seg}^{ads,out}$		
Variables	r	Strength	p-value	r	Strength	p-value
N_{block}	0.094	Very weak	0.377	0.091	Very weak	0.393
$\|Z_{net}\|$	-0.171	Very weak	0.106	-0.208	Weak	0.048
R_{core}	-0.108	Very weak	0.306	0.003	Very weak	0.978
N_{mon}	-0.196	Very weak	0.063	0.219	Weak	0.037
Z_{net}	0.053	Very weak	0.619	0.463	Moderate	0.000
pH	-0.208	Weak	0.048	-0.294	Weak	0.005

Both scatter plots and r coefficients show all variables generally have (very) weak correlation with $N_{seg}^{ads,in}$, and $N_{seg}^{ads,out}$ (see Table 4.3 and figure 4.19). This is a different result from correlation analysis of R_g, which shows a very high correlation with $|Z_{net}|$ and a very low correlation with pH. pH is the only significant variable which is correlated to $N_{seg}^{ads,in}$.

Furthermore, scatter plots show that high value of $N_{seg}^{ads,in}$ and low value near zero appear to be separated as different groups for all variables generally, whereas $N_{seg}^{ads,out}$ does not.

There may be a main factor, which is not considered here (missing variable), determining the two groups of $N_{seg}^{ads,in}$. The presence of a kinetic trap associated with an insufficient sampling can be one of these factors. Furthermore, It can be more appropriate to represent the occupation of the PE inside the HNT using a categorical variables rather than the continuous variables by looking at discret pattern.

To sum up, although these results of correlation analysis can not give a conclusive solution to estimate the utility of adsorption of PE onto the HNT in terms of immobilization and encapsulation, they are meaningful in the perspective that we can infer how to improve simulations by adding or transforming variables.

Chapter 5

Conclusion

This thesis show that Monte Carlo simulations of a HNT and a PE using a CG model was successfully implemented. It was demonstrated that pH-dependent characteristic of HNT obtained in the simulation has a good qualitative match to experimental work. Conformational and adsorptional behaviors of the PE was investigated from the perspective of the surface characteristic of the HNT.

pH-dependent characteristic of the HNT was identified by comparing titration curves, which showed a similar tendency compared to results from experiments. The size of the pH-independent PE was found to vary with change in pH. Increase of pH induces a decrease in a negatively charged PE, but the opposite for positively charged PE. Contact and adsorption analysis also showed different results for the two PEs. This behavior was discussed in terms of the interaction with the HNT *i.e.* adsorption, and in terms of indirect effect by screening of the counterions.

Negatively charged PE showed adsorption onto the outer surface for low pH values which was found to be likely a kinetic trap. Further simulations revealed that a PE generated inside the HNT show a lower energy than the conformation where it is adsorbed on the outer surface. In addition, density distributions showed that the PE occupies preferably the center of the HNT, if one looks at the dimension along the HNT. Regarding the radial distribution of the monomers the PE tends to slightly accumulate at the inner wall at low pH values. At higher pH the radial distribution is more uniform and adsorption to the inner surface decreases.

Statistical analysis of data obtained from simulations with varying architectures of PE and pH conditions is performed. Several structural features: number of blocks, absolute value of net charge, and core ratio were shown to be closely correlated to PE condensation. Interestingly, adsorption of the PE was not significantly correlated to either of the five characteristics of PE, but was correlated to pH. The number of segments in contact with the inside and outside of the HNT indicated a need to add or replace variables in the existing data. The presented statistical analysis shows potential for predicting PE conformation and adsorption to HNT from the simulation results.

In conclusion, the HNTs appear to be a promising carrier for enzyme immobilization by adsorption but challenges on encapsulating these in the HNTs lumen may arise.

Chapter 6

Future works

From the perspective of models and simulations, errors from a mismatch of experimental data can reduce the accuracy of the simulations. When modelling HNT, one that was not considered was the specific properties of the side or edge of the HNT. Therefore, special modeling for these two areas is required, for example, reordering beads. A second point is the characterization of the wall of the HNT. Here, it is simply described with the same dielectric constant of water but this is probably not correct. The dielecric constant of the HNT wall may affect significantly the electrostatic properties of the surfaces. Therefore, given that the main characteristic of HNT is electrical characteristics of surfaces, it may be an important factor to consider, and runs including these terms are recommended.

When describing radius of gyration variation of PE according to pH, we refer to the structural features of the tube, *e.g.* diameter or curvature. We suggest varying these features. In particular, for PE adsorbing on the inner surface, the diameter and the size of the PE may be important because it should first have access to the lumen. On the other hand, when describing the screening effect of the counterions for structural reasons, it is described as a change in the total amount of charge from free ions. This result is more intuitive if the tube with only one type of surface group is studied and it is investigated how effectively charge works for screening.

To find a statistically significant factor, it is difficult to establish a predictive model because the data we have is not normally distributed. Therefore, it is suggested to add data to satisfy the normal distribution by performing more runs with diversified variables. When

normality is satisfied, Pearson's correlation analysis can be studied and the establishment of multiple linear regression model for estimating R_g, $\left\langle N_{\mathrm{seg}}^{\mathrm{ads,in}} \right\rangle$ and $\left\langle N_{\mathrm{seg}}^{\mathrm{ads,out}} \right\rangle$ is also possible. On the other hand, if this method takes to much time to simulate, it is recommended to establish a nonlinear regression model, such as Kerner regression or logistic regression model.

Bibliography

[1] A Zaks and DR Dodds. Biotransformations in the discovery and development of pharmaceuticals. *Current opinion in drug discovery & development*, 1(3):290–303, 1998.

[2] Jian Zhong Jin and Jie Zhang. Highly enantioselective hydrolysis of racemic isopropyl tert-leucinate by newly discovered baclicus lincheniformis jx010 for synthesis of l-tert-butyl leucine. In *Advanced Materials Research*, volume 343, pages 453–456. Trans Tech Publ, 2012.

[3] Rolf D Schmid and Robert Verger. Lipases: interfacial enzymes with attractive applications. *Angewandte Chemie International Edition*, 37(12):1608–1633, 1998.

[4] Yuko Ogushi, Shinji Sakai, and Koei Kawakami. Synthesis of enzymatically-gellable carboxymethylcellulose for biomedical applications. *Journal of bioscience and bioengineering*, 104(1):30–33, 2007.

[5] Pennina R Langer, Alex A Waldrop, and David C Ward. Enzymatic synthesis of biotin-labeled polynucleotides: novel nucleic acid affinity probes. *Proceedings of the National Academy of Sciences*, 78(11):6633–6637, 1981.

[6] Nemanja Miletić, Aleksandra Nastasović, and Katja Loos. Immobilization of biocatalysts for enzymatic polymerizations: possibilities, advantages, applications. *Bioresource Technology*, 115:126–135, 2012.

[7] Narges Nobakht, Mohammad Ali Faramarzi, Abbas Shafiee, Mehdi Khoobi, and Ezzat Rafiee. Polyoxometalate-metal organic framework-lipase: An efficient green catalyst for synthesis of benzyl cinnamate by enzymatic esterification of cinnamic acid. *International journal of biological macromolecules*, 113:8–19, 2018.

[8] C Tudisco, G Zolubas, B Seoane, HR Zafarani, M Kazemzad, J Gascon, P-L Hagedoorn, and L Rassaei. Covalent immobilization of glucose oxidase on amino mofs via post-synthetic modification. *RSC Advances*, 6(109):108051–108055, 2016.

[9] Sizhu Ren, Yuxiao Feng, Huan Wen, Conghai Li, Baoting Sun, Jiandong Cui, and Shiru Jia. Immobilized carbonic anhydrase on mesoporous cruciate flower-like metal organic framework for promoting co2 sequestration. *International journal of biological macromolecules*, 117:189–198, 2018.

[10] Muhammad Bilal, Muhammad Adeel, Tahir Rasheed, and Hafiz MN Iqbal. Multifunctional metal–organic frameworks-based biocatalytic platforms: Recent developments and future prospects. *Journal of Materials Research and Technology*, 2019.

[11] Sandro Matosevic, Nicolas Szita, and Frank Baganz. Fundamentals and applications of immobilized microfluidic enzymatic reactors. *Journal of Chemical Technology & Biotechnology*, 86(3):325–334, 2011.

[12] Jana Křenková and František Foret. Immobilized microfluidic enzymatic reactors. *Electrophoresis*, 25(21-22):3550–3563, 2004.

[13] Shakeel Ahmed Ansari and Qayyum Husain. Potential applications of enzymes immobilized on/in nano materials: A review. *Biotechnology advances*, 30(3):512–523, 2012.

[14] Teofil Jesionowski, Jakub Zdarta, and Barbara Krajewska. Enzyme immobilization by adsorption: A review. *Adsorption*, 20(5-6):801–821, 2014.

[15] Mengfan Wang, Wei Qi, Rongxin Su, and Zhimin He. Advances in carrier-bound and carrier-free immobilized nanobiocatalysts. *Chemical Engineering Science*, 135: 21–32, 2015.

[16] Shilin Cao, Pei Xu, Yongzheng Ma, Xiaoxiao Yao, Yuan Yao, Minhua Zong, Xuehui Li, and Wenyong Lou. Recent advances in immobilized enzymes on nanocarriers. *Chinese Journal of Catalysis*, 37(11):1814–1823, 2016.

[17] Xihui Yin, Vishal Gupta, Hao Du, Xuming Wang, and Jan D Miller. Surface charge and wetting characteristics of layered silicate minerals. *Advances in Colloid and Interface Science*, 179:43–50, 2012.

[18] Clemente Bretti, Salvatore Cataldo, Antonio Gianguzza, Gabriele Lando, Giuseppe Lazzara, Alberto Pettignano, and Silvio Sammartano. Thermodynamics of proton binding of halloysite nanotubes. *The Journal of Physical Chemistry C*, 120(14): 7849–7859, 2016.

[19] Rui Zhai, Bing Zhang, Lin Liu, Yinde Xie, Haoqin Zhang, and Jindun Liu. Immobilization of enzyme biocatalyst on natural halloysite nanotubes. *Catalysis Communications*, 12(4):259–263, 2010.

[20] Maxime Delhorme, Christophe Labbez, Céline Caillet, and Fabien Thomas. Acid-base properties of 2: 1 clays. i. modeling the role of electrostatics. *Langmuir*, 26(12): 9240–9249, 2010.

[21] Francesco Ferrante, Nerina Armata, and Giuseppe Lazzara. Modeling of the halloysite spiral nanotube. *The Journal of Physical Chemistry C*, 119(29):16700–16707, 2015.

[22] Jeff Hardin, Gregory Paul Bertoni, and Lewis J Kleinsmith. *Becker's World of the Cell*. Pearson Higher Ed, 2017.

[23] Magnus Kjaergaard and Birthe B Kragelund. Functions of intrinsic disorder in transmembrane proteins. *Cellular and Molecular Life Sciences*, 74(17):3205–3224, 2017.

[24] Barbara Zambelli, Nunilo Cremades, Paolo Neyroz, Paola Turano, Vladimir N Uversky, and Stefano Ciurli. Insights in the (un) structural organization of bacillus pasteurii ureg, an intrinsically disordered gtpase enzyme. *Molecular BioSystems*, 8(1): 220–228, 2012.

[25] Peter E Wright and H Jane Dyson. Intrinsically disordered proteins in cellular signalling and regulation. *Nature reviews Molecular cell biology*, 16(1):18, 2015.

[26] Peng Yuan, Daoyong Tan, and Faïza Annabi-Bergaya. Properties and applications of halloysite nanotubes: recent research advances and future prospects. *Applied Clay Science*, 112:75–93, 2015.

[27] C. DeArmitt Phantom Plastic. Halloysite clay nanotubes. https://phantomplastics.com/functional-fillers/halloysite/, 2012 (accessed on June 2019).

[28] Proteinwiki. List of electronegativity values of the elements. https://sciencenotes.org/list-of-electronegativity-values-of-the-elements/, May 9, 2015 (updated on December 8, 2018 ; accessed on June 2019).

[29] Michele Vacatello. Monte carlo simulations of polymer melts filled with solid nanoparticles. *Macromolecules*, 34(6):1946–1952, 2001.

[30] Andreia F Jorge, Rita S Dias, and Alberto ACC Pais. Enhanced condensation and facilitated release of dna using mixed cationic agents: a combined experimental and monte carlo study. *Biomacromolecules*, 13(10):3151–3161, 2012.

[31] Michael King. Development of a coarse-grained model for calcium minerals. https://www.chemie.uni-konstanz.de/ag-peter/research/research-projects/material-science-related-topics/biomineralization/development-of-a-coarse-grained-model-for-calcium-minerals/, 2012 (accessed on June 2019).

[32] Peng Yuan, Peter D Southon, Zongwen Liu, Malcolm ER Green, James M Hook, Sarah J Antill, and Cameron J Kepert. Functionalization of halloysite clay nanotubes by grafting with γ-aminopropyltriethoxysilane. *The Journal of Physical Chemistry C*, 112(40):15742–15751, 2008.

[33] Pooria Pasbakhsh, G Jock Churchman, and John L Keeling. Characterisation of properties of various halloysites relevant to their use as nanotubes and microfibre fillers. *Applied Clay Science*, 74:47–57, 2013.

[34] Jean-Pierre Morel, Nicolas Marmier, Charlotte Hurel, and Nicole Morel-Desrosiers. Acid–base properties of the alumina surface: Influence of the titration procedures

on the microcalorimetric results. *Journal of colloid and interface science*, 338(1): 10–15, 2009.

[35] Peter Tompa. Intrinsically unstructured proteins. *Trends in biochemical sciences*, 27 (10):527–533, 2002.

[36] Leah4sci. Finding charge on amino acids in preparation for isoelectric point calculations. http://leah4sci.com/amino-acid-charge-in-zwitterions-and-isoelectric-point-mcat-tutorial/, accessed June, 2019.

[37] Proteinwiki. Intrinsically disordered protein. https://proteopedia.org/wiki/index.php/Intrinsically_Disordered_Protein, accessed June, 2019.

[38] U.S. National Library of Medicine National Center for Biotechnology Information. Glutathione. https://pubchem.ncbi.nlm.nih.gov/compound/GLUTATHIONE, accessed June, 2019.

[39] Reščič Jurij and Linse Per. Molsim: A modular molecular simulation software. *Journal of computational chemistry*, 36(16):1259–1274, 2015.

[40] Ideal chain model : Wikipedia. Ideal chain model. https://en.wikipedia.org/wiki/Ideal_chain#cite_ref-1, accessed June, 2019.

[41] Rita de Sousa Dias, Stine Nalum Nss, Arne Mikkelsen, and Arnljot Elgster. *MOLECULAR BIOPHYSICS - Compendium*. NTNU, 2017.

[42] Jun Araki. Electrostatic or steric?–preparations and characterizations of well-dispersed systems containing rod-like nanowhiskers of crystalline polysaccharides. *Soft Matter*, 9(16):4125–4141, 2013.

[43] Anand VP Gurumoorthy and KH Khan. Polymers at interfaces: biological and non-biological applications. *Recent Research in Science and Technology*, 3(2), 2011.

[44] Norman H Nie, Dale H Bent, and C Hadlai Hull. *SPSS: Statistical package for the social sciences*, volume 227. McGraw-Hill New York, 1975.

[45] Bernard Rosner. Fundamentals of biostatistics. ed. *Australia: Duxbury*, 2000.

[46] Robert V Hogg, Joseph McKean, and Allen T Craig. *Introduction to mathematical statistics*. Pearson Education, 2005.

[47] Andy Field. *Discovering statistics using IBM SPSS statistics*. sage, 2013.

[48] Kassambara. Plot multivariate continuous data. http://www.sthda.com/english/articles/32-r-graphics-essentials/130-plot-multivariate-continuous-data/, 17 Nov 2017 (accessed on June 2019).

[49] Haldun Akoglu. User's guide to correlation coefficients. *Turkish journal of emergency medicine*, 2018.

[50] Phanny ITH. Guideline for interpreting correlation coefficient. https://www.slideshare.net/phannithrupp/guideline-for-interpreting-correlation-coefficient, Jul 5, 2014 (accessed on June 2019).

[51] Alfred P Rovai, Jason D Baker, and Michael K Ponton. *Social science research design and statistics: A practitioner's guide to research methods and IBM SPSS*. Watertree Press LLC, 2013.

[52] Dragonite¢ for Controlled Release of Active Agents. Leading global producer of halloysite clay. http://appliedminerals.com/images/uploads/controlled-release/Applied_Minerals_-_Controlled_Release_Presentation_--.pdf, 2010 (accessed on June 2019).

[53] Giuseppe Lazzara, Marina Massaro, and Serena Riela. Current status of nanoclay phytotoxicity. In *Phytotoxicity of Nanoparticles*, pages 151–174. Springer, 2018.

[54] John R Holum and Sandra L Olmsted. *Fundamentals of general, organic, and biological chemistry*. John Wiley & Sons New York, 1994.

[55] LibreTexts Chemistry. 15.6: Acid-base titration curves. https://chem.libretexts.org/Bookshelves/General_Chemistry/Map%3A_Principles_of_Modern_Chemistry_(Oxtoby_et_al.)/UNIT_4%3A_EQUILIBRIUM_IN_CHEMICAL_REACTIONS/15%3A_Acid%E2%80%93Base_Equilibria/15.6%3A_Acid-Base_Titration_Curves, updated 19 Jan 2019 (accessed on June 2019).

[56] Gilbert Newton Lewis. *Valence and the Structure of Atoms and Molecules*. Number 14. Chemical Catalog Company, Incorporated, 1923.

[57] Andy Schmitz. *Principles of General Chemistry*. Number v1.0. Creative Commons, December 29, 2012.

[58] Morten Stornes, Per Linse, and Rita S Dias. Monte carlo simulations of complexation between weak polyelectrolytes and a charged nanoparticle. influence of polyelectrolyte chain length and concentration. *Macromolecules*, 50(15):5978–5988, 2017.

[59] OV Borisov, EB Zhulina, and TM Birshtein. Diagram of the states of a grafted polyelectrolyte layer. *Macromolecules*, 27(17):4795–4803, 1994.

[60] EB Zhulina, J Klein Wolterink, and OV Borisov. Screening effects in a polyelectrolyte brush: Self-consistent-field theory. *Macromolecules*, 33(13):4945–4953, 2000.

[61] Daniel George Angelescu, Robijn Bruinsma, and Per Linse. Monte carlo simulations of polyelectrolytes inside viral capsids. *Physical Review E*, 73(4):041921, 2006.

[62] David J Griffiths. Introduction to electrodynamics, 2005.

Appendix

6.1 Normality test of $\left\langle R_g^2 \right\rangle^{1/2}$

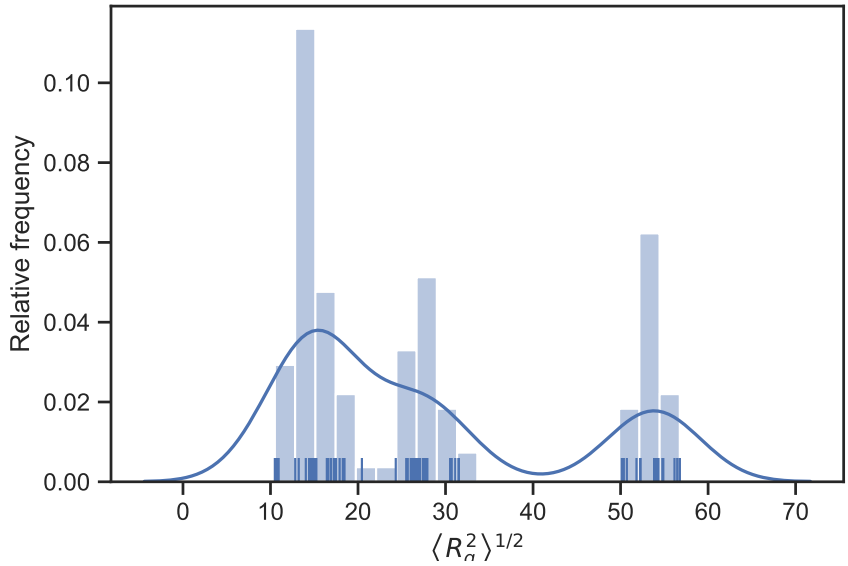

Figure 6.1: Histogram of $\left\langle R_g^2 \right\rangle^{1/2}$.

Table 6.1: Tests of normality for $\left\langle R_g^2 \right\rangle^{1/2}$. *a* refers the Kolmogorov-Smirnov test and *b* refers Shapiro-Wilk test.

Variable	Statistic	df	p-value
$\left\langle R_g^2 \right\rangle^{1/2}$	0.217	91	0.000^a
$\left\langle R_g^2 \right\rangle^{1/2}$	0.792	91	0.000^b

6.2 Normality test of $N_{\text{seg}}^{\text{ads,in}}$ and $N_{\text{seg}}^{\text{ads,out}}$

Table 6.2: Tests of normality for $N_{\text{seg}}^{\text{ads,in}}$ and $N_{\text{seg}}^{\text{ads,out}}$. *a* refers the Kolmogorov-Smirnov test and *b* refers Shapiro-Wilk test.

Variable	Statistic	df	p-value
$N_{\text{seg}}^{\text{ads,in}}$	0.506	91	0.000^{a}
$N_{\text{seg}}^{\text{ads,in}}$	0.455	91	0.000^{b}
$N_{\text{seg}}^{\text{ads,out}}$	0.249	91	0.000^{a}
$N_{\text{seg}}^{\text{ads,out}}$	0.691	91	0.000^{b}